












TanDEM-X: 10 Years of Formation Flying Bistatic SAR Interferometry

Manfred Zink , Alberto Moreira , *Fellow, IEEE*, Irena Hajnsek , *Fellow, IEEE*, Paola Rizzoli , Markus Bachmann , Ralph Kahle , Thomas Fritz , Martin Huber , Gerhard Krieger , *Fellow, IEEE*, Marie Lachaise , Michele Martone , Edith Maurer, and Birgit Wessel

Abstract—On June 21, 2010, the TanDEM-X mission was launched and opened a new era in spaceborne radar remote sensing. The first formation flying radar system was built by extending the TerraSAR-X synthetic aperture radar (SAR) mission by a second, TerraSAR-X-like satellite TanDEM-X. The resulting large single-pass SAR interferometer features flexible baseline selection, enabling the acquisition of highly accurate cross-track interferograms not impacted by temporal decorrelation and atmospheric disturbances. The primary objective of the mission was the generation of a global Digital Elevation Model (DEM) with unprecedented accuracy (12-m horizontal resolution and 2-m relative height accuracy). The main mission phase for DEM data acquisition has been finished in 2014; the processing of the global TanDEM-X DEM was concluded in September 2016. The final DEM product is well within specifications and features an extremely low percentage of void areas. It is of fundamental importance for a wide range of commercial and scientific applications. But the scientific exploitation of TanDEM-X is not limited to the DEM. TanDEM-X has unique capabilities, including along-track interferometry, and new bistatic and multistatic SAR techniques, that support numerous secondary mission objectives. Indeed, some of these experiments were directly performed during the DEM acquisition phase, when suitable satellite formation geometries were available. Moreover, regular acquisitions over selected super test sites enabled multitemporal analyses. A dedicated science phase after the DEM acquisitions included up to 4 km cross-track baselines, operation in the so-called Dual-Receive Antenna mode, as well as a period in pursuit monostatic flight formation. Comparisons of the TanDEM-X DEM with that of SRTM, or among multitemporal TanDEM-X data, revealed dramatic, ongoing, changes in Earth’s topography, especially over ice and forests. In the last 3.5 years the mission has further acquired data for a global change layer showing the height changes relative to the first global DEM dataset. The so-called “Change DEM” is planned for release in 2021. Despite being well beyond their design lifetime, both satellites are still fully functional and have enough consumables for several additional years. Therefore, bistatic operations continue with a focus on changes in the cryosphere, biosphere, and densely populated urban areas.

Index Terms—Bistatic SAR, digital elevation model (DEM), formation flight, interferometry, spaceborne SAR, synthetic aperture radar (SAR).

I. INTRODUCTION

SPACEBORNE SAR interferometry is a key technique for topographic mapping. Early demonstrations have been performed with single satellites acquiring image pairs at time intervals given by the orbit repeat cycle. Temporal decorrelation and variations in atmospheric conditions limit the achievable accuracy of the so-called repeat-pass interferometry. In 2000 the Shuttle Radar Topography Mission (SRTM) [1] overcame these limitations by supplementing each of the SIR-C and X-SAR radar instruments [2] by a second receive channel, as well as a second receive-only antenna at the end of a 60 m long deployable mast forming the first single-pass SAR interferometer in space. In 11 days SRTM collected data for generation of a DEM, covering the Earth’s surface between -56° and $+60^\circ$ latitude, at 30 and 90 m posting, and 10 m height accuracy. This near global dataset became a worldwide standard and one of the most used remote sensing dataset so far. The very successful cooperation between NASA/JPL and DLR on the Shuttle Radar Missions paved the way for the development of TerraSAR-X and TanDEM-X.

The TanDEM-X (TerraSAR-X add-on for Digital Elevation Measurements) mission concept is based on the two synthetic aperture radar (SAR) satellites, TerraSAR-X and TanDEM-X, operating as the first formation-flying bistatic SAR interferometer in space [3]. Since October 2010, the two satellites have been orbiting the Earth at an altitude of 514 km (at the equator) in a so-called Helix formation at typical distances between 120 and 500 m, as illustrated in Fig. 1. Images are nominally acquired in a bistatic configuration, where one satellite transmits and both simultaneously receive the backscattered signal from Earth’s surface. Avoiding temporal and atmospheric decorrelation enables the acquisition of highly accurate interferograms as input to the DEM generation. A dedicated acquisition strategy has been developed and optimized throughout the years, in order to achieve the desired performance on a global scale.

The global TanDEM-X DEM has been defined to meet or exceed the specifications presented in Table I [4]. The height values are referred to the WGS84 ellipsoid and the coverage must reach at least 97% of all land masses, i.e., at most 3% of

Manuscript received November 6, 2020; revised December 21, 2020 and January 22, 2021; accepted February 11, 2021. Date of publication February 26, 2021; date of current version April 7, 2021. (*Corresponding author: Manfred Zink.*)

The authors are with the German Aerospace Center (DLR), Wessling 82230, Germany (e-mail: manfred.zink@dlr.de; alberto.moreira@dlr.de; irena.hajnsek@dlr.de; paola.rizzoli@dlr.de; markus.bachmann@dlr.de; ralph.kahle@dlr.de; thomas.fritz@dlr.de; martin.huber@dlr.de; gerhard.krieger@dlr.de; marie.lachaise@dlr.de; michele.martone@dlr.de; edith.maurer@dlr.de; birgit.wessel@dlr.de).

Digital Object Identifier 10.1109/JSTARS.2021.3062286

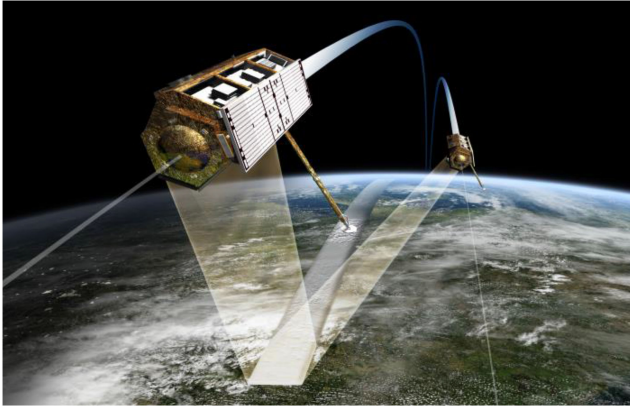


Fig. 1. Since 2010 TerraSAR-X and TanDEM-X have been flying in close formation operating as a bistatic radar interferometer.

TABLE I
SPECIFICATION OF THE GLOBAL TANDEM-X DEM

Parameter	Definition	Requirement
Relative Vertical Accuracy	90% linear point-to-point error in $1^\circ \times 1^\circ$ cell	2 m (slope < 20%) 4 m (slope > 20%)
Absolute Vertical Accuracy	90% linear error	10 m
Spatial Resolution	independent pixels	12 m (0.4 arc sec)

all DEM pixels over dry land (water bodies excluded) might be flagged as void or invalid (e.g., due to acquisition gaps, low signal quality, shadow or layover effects). All heights represent the reflective surface at X-band, i.e., the global DEM is a surface model. Depending on their properties, the elevation for forests lies commonly in the upper canopy region. For dense forests, such as tropical rainforests, it approximates the top of the canopy, while the penetration increases to several meters with decreasing density. Over snow- and ice-covered regions, similar penetration phenomena occur, depending on the snow pack temperature, density and microstructure. Here penetration can reach up to 8 m, as reported in [5] for TanDEM-X acquisitions over Greenland.

Beyond the primary mission goal of generating the global DEM, TanDEM-X supports applications based on along-track interferometry and the demonstration and application of new SAR techniques, with a focus on multistatic SAR, polarimetric SAR interferometry, digital beamforming, and super resolution. Both radar instruments feature a very flexible commanding scheme, which in combination with the adjustable baseline geometries enables hitherto unprecedented capabilities for experimental modes and new techniques.

The following sections provide an overview of the mission concept and key TanDEM-X features, like the Helix formation, the system synchronization, and the global acquisition strategy. A description of the interferometric calibration and of the DEM processing chain in Section IV and Section V, respectively, is

followed by a summary of the DEM performance in Section VI. This article concludes with a short overview on the achievements beyond the global DEM and conclusions including an outlook to follow-on missions.

II. MISSION CONCEPT

The TanDEM-X mission is an extension of the TerraSAR-X radar mission [6], co-flying a second almost identical satellite in a close formation. The TerraSAR-X satellite (TSX), as basis for TanDEM-X, was successfully launched into a 514 km, 11-day repeat cycle, sun-synchronous dusk-dawn orbit on June 15, 2007. Late in the development, necessary features required for the TanDEM-X mission were implemented on TSX. Examples are additional X-band horn antennas for intersatellite phase synchronization, a dual-frequency GPS receiver for precise orbit and baseline determination, improved radio frequency phase stability of the SAR instrument, and pulse repetition frequency synchronization based on GPS as a common time reference. The second satellite (TDX, launched on June 21, 2010) is mostly a rebuild of TSX with only minor modifications like an additional cold gas propulsion system for formation fine tuning, double-sized on-board solid-state memory for increased data recording capacity, and an additional S-band receiver to enable the reception of telemetry and GPS position information broadcast by TSX. The instruments on both satellites are advanced high-resolution X-band (center frequency 9.65 GHz, chirp bandwidth up to 300 MHz) synthetic aperture radars, which can be operated in Spotlight, Stripmap, and ScanSAR mode with full polarization capability [7].

Flying at a typical distance of a few hundred meters, the two satellites perform single-pass interferometry and acquire cross-track interferograms. By evaluating the phase difference between two coherent radar signals acquired from slightly different spatial positions, TanDEM-X is able to measure the range difference Δr between the two satellites and a given scatterer on the ground with millimetric precision. The height of the scatterer is inferred from this range difference by geometric triangulation. The sensitivity of the phase-to-height scaling depends on the distance B between the two satellites, known as the baseline. As the component of B perpendicular to the line of sight, B_\perp , increases, the sensitivity of the radar interferometer to small height variations also increases. Thus, a large B_\perp increases the height acuity, but can lead to problems in interpreting the mapping of phase differences to height, which is ambiguous with the wavelength. A convenient measure of height acuity is the so-called height of ambiguity defined as follows:

$$h_{\text{amb}} = \frac{\lambda r_0 \sin(\theta_i)}{B_\perp} \quad (1)$$

where λ is the wavelength, r_0 the slant range from the satellites to the scatterer under consideration, and θ_i the local incidence angle of the electromagnetic wave. For TanDEM-X, it was necessary to design the observation campaigns with values of h_{amb} that would balance height acuity with phase disambiguation.



Fig. 2. Helix satellite formation. Red: TSX, Green: TDX; Typical baseline values vary from 120 to 500 m.

A. Orbit Configuration and Formation Flying

The TanDEM-X operational scenario requires the coordinated operation of two satellites flying in close formation. The so-called Helix formation combines an out-of-plane (horizontal) orbital displacement by small differences in the right ascension of the ascending nodes with a radial (vertical) separation by different eccentricity vectors resulting in a helix-like relative movement of the satellites along the orbit, as sketched in Fig. 2. Since the two orbits never cross (i.e., the combined horizontal/radial separation is always larger than 120 m), arbitrary shifts and drifts of the satellites along their orbits are allowed. This enables safe spacecraft operation without the necessity for autonomous control.

For a complete mapping of the Earth with dedicated heights of ambiguity, the Helix formation parameters, namely the horizontal and vertical distances between the satellites and the so-called phase of libration [8], are regularly adjusted. Southern and northern latitudes can be mapped with the same formation by using ascending orbits for one hemisphere and descending orbits for the other.

The satellite orbits are controlled according to the relative eccentricity/inclination vector control concept [8], where daily maneuver pairs compensate for the differential forces acting on the formation (mainly due to Earth oblateness and small deviations of previous orbit control maneuvers when compared to the nominal orbit position). Since the close formation was initiated in October 2010 [9], the formation geometry has been subject to frequent changes as implied by the TanDEM-X acquisition plan. Fig. 3 depicts all target formation geometries realized during the first four years, which also featured two changes in the direction of relative motion between the satellites, so-called swaps [10].

After ten years of formation flying, the two satellites have reliably and precisely executed almost 10 000 orbit control maneuvers, mainly for formation reconfiguration and maintenance, but also for TSX orbit control and debris collision avoidance. At an orbital velocity of 27 400 km/h, the achieved control accuracy in cross-track 2-D is below 5 m

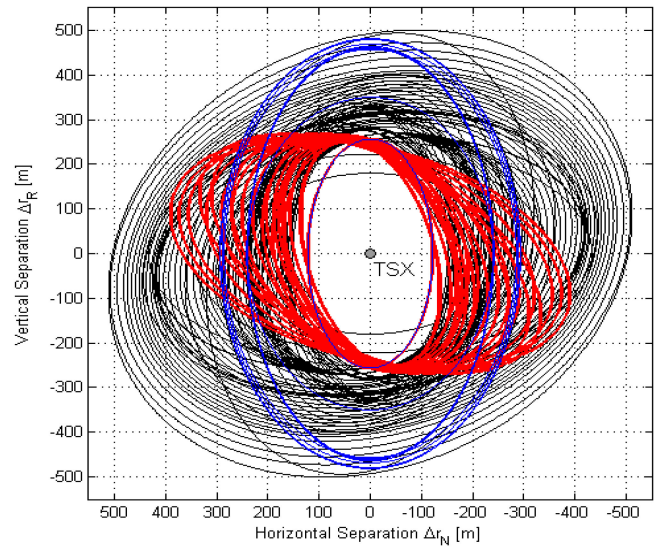


Fig. 3. TDX-TSX relative orbits during the main mission phase. TSX is located in the center of the coordinate system; the ellipses describe TDX's motion with respect to TSX in the plane perpendicular to flight direction. Counter-clockwise rotation in period 10/2010–08/2013 (black), swap and clockwise rotation (red), and re-swap to counter-clockwise rotation in period 04–09/2014 (blue).

(RMS) for stable geometries and below 10 m for horizontally drifting formations, and 30 m (1-D, RMS) in along-track direction.

B. Interferometric Configurations and Acquisition Modes

TanDEM-X can acquire interferometric data in different configurations [3], [4]: examples are the bistatic, pursuit monostatic, and alternating bistatic modes. The different interferometric configurations can be further combined with different TSX and TDX SAR imaging modes like Stripmap, ScanSAR, and Spotlight. Operational DEM generation is performed using the bistatic Stripmap mode in single polarization (HH). This mode uses either TSX or TDX as a transmitter (depending on the resources available in each satellite) to illuminate a common radar footprint on the Earth's surface. The scattered signal is then recorded by both satellites simultaneously. This simultaneous data acquisition makes dual use of the available transmit power and the range from the transmitting satellite to the target is identical in both measurements. Therefore, the interferometric phase changes are only due to the one-way range distance difference of the backscattered signals to TSX and TDX, respectively, halving the phase sensitivity of the bistatic operation when compared to the pursuit monostatic (i.e., repeat-pass) acquisition.

C. System Synchronization

A peculiarity of the bistatic data acquisition is the use of independent oscillators for the modulation and demodulation of the radar pulses. Any deviation between the two oscillators causes residual modulations of the recorded azimuth signal. The impact of oscillator phase noise in bistatic SAR has been analyzed in [11] where it is shown that oscillator noise may cause significant errors in both the interferometric phase and SAR focusing.

The stringent requirements for interferometric phase stability in the bistatic mode hence require an appropriate relative phase referencing between the two SAR instruments. For TanDEM-X, a dedicated intersatellite X-band synchronization link has been established: the nominal bistatic SAR data acquisition is briefly interrupted, and radar pulses are exchanged between the two satellites using dedicated synchronization horn antennas. On ground, a correction signal can be derived from the recorded synchronization pulses. This compensates the oscillator-induced phase errors in the bistatic SAR signal to be better than 1° [12], corresponding to height errors in the decimeter range.

III. DATA ACQUISITION STRATEGY AND OPTIMIZATION

The acquisition strategy to generate the global DEM has been driven by the product specification for the relative height accuracy, which is in turn directly related to the phase noise that can be quantified through the interferometric coherence, and the perpendicular baseline or, equivalently, the height of ambiguity [13]. The latter needs, on one hand, to be sufficiently small to ensure the specification fulfillment on global scale, and, on the other hand, it must be large enough to guarantee a robust phase unwrapping process [14].

The interferometric coherence of the acquired data quantifies the amount of noise affecting the interferogram and is the key parameter for assessing its quality. It has been monitored throughout the entire mission and has served as a trigger parameter for optimizing the global acquisition strategy [15]. It comprises all decorrelation sources such as signal-to-noise ratio, quantization, ambiguities, baseline decorrelation, volume decorrelation, and temporal decorrelation [16], [17].

Depending on the particular land cover, terrain characteristics of the area under illumination, and the specific acquisition geometry used for the data take, several error contributions may affect the quality of an interferometric SAR (InSAR) DEM [18].

- 1) *High-Relief Terrain*: SAR acquisitions over steep and irregular surfaces are often affected by geometric distortions such as shadow and layover. In most cases, a reacquisition of the affected area using a different observation geometry mitigates such effects.
- 2) *Forested Areas*: Over vegetated areas the presence of multiple scatterers at different heights within a single resolution cell causes volume decorrelation impacting the DEM quality. Optimized acquisitions using smaller baselines reduce these effects [19], [20].
- 3) *Snow and Ice*: Similar to vegetated areas, dry snow/ice-covered regions are also characterized by volume decorrelation [5].
- 4) *Sandy Deserts*: The quality of SAR surveys over dry sandy regions is strongly affected by the weak backscattered returns mainly due to absorption of the radar pulses. Steeper incidence angles result in an increased backscatter and, consequently, a higher signal-to-noise ratio and coherence [21], [22], as shown in Fig. 4.
- 5) *Phase Unwrapping Errors*: These are often the most prominent errors in interferometric DEM processing. The

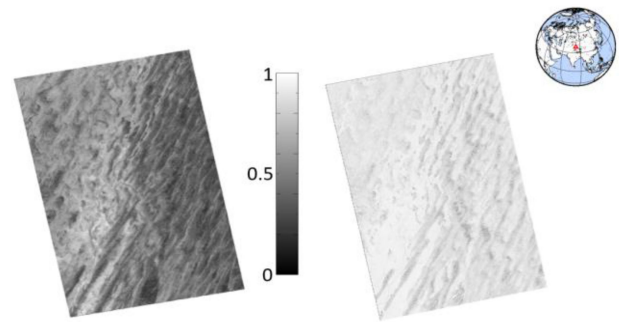


Fig. 4. TanDEM-X coherence maps over Taklamakan desert (China); (left) HH polarization, : 48° , mean coherence: 0.52; (right) HH polarization, mean incidence angle: 16° , mean coherence: 0.84.

application of an incorrect ambiguity cycle in phase-to-height reconstruction may lift or lower entire regions by integer multiples of the height of ambiguity value. To achieve robust phase unwrapping, two TanDEM-X acquisitions with different baselines have been systematically combined in ground processing [23]–[25].

Nominal DEM acquisitions were performed in right-looking observation mode in ascending/descending orbits over the Northern and Southern hemisphere, respectively. In order to prevent the satellites from irradiating and potentially damaging each other, the so-called exclusion zones have been defined, which constrain the portions of the orbit in which the individual satellites can be either active or passive for bistatic data takes.

The sequence of mission phases is shown in Fig. 5. In the first year of operation—from December 2010 to March 2012—a global acquisition of Earth’s landmasses excluding Antarctica was carried out. According to the acquisition strategy, the orbit formation was properly set in order to keep a height of ambiguity of about 50 m for all different incidence angles and latitudes. The Helix formation was continuously reconfigured (see Fig. 6). To allow reliable phase unwrapping, additional acquisitions were performed over densely forested areas (e.g., over the Amazon rainforest in Brazil or the tropical forest in South East Asia) and over mountainous regions. For this reason, acquisitions with a height of ambiguity typically larger than 60 m, hence requiring smaller baselines, were commanded [26], [27].

The acquisitions of the second global coverage started in April 2012 and lasted until April 2013 [28]–[31]. The target height of ambiguity was reduced from 50 to 35 m, where a decrease by a factor of 0.7 was empirically found to be optimal to combine the two acquisitions for the exploitation of dual-baseline phase unwrapping algorithms and for the overall improvement of the relative height accuracy [23], [24], [32]–[34]. The two global coverages were performed using swath positions shifted against each other by half of the swath width to reduce the impact of SNR degradation at the swath edges, resulting in homogeneous height performance over the whole access range [35], [36]. In addition, the quantization rates were also finetuned to optimize the tradeoff between interferometric SAR performance and data volume [16], [37]. Continuous performance analysis and monitoring during the first two years suggested the need to perform

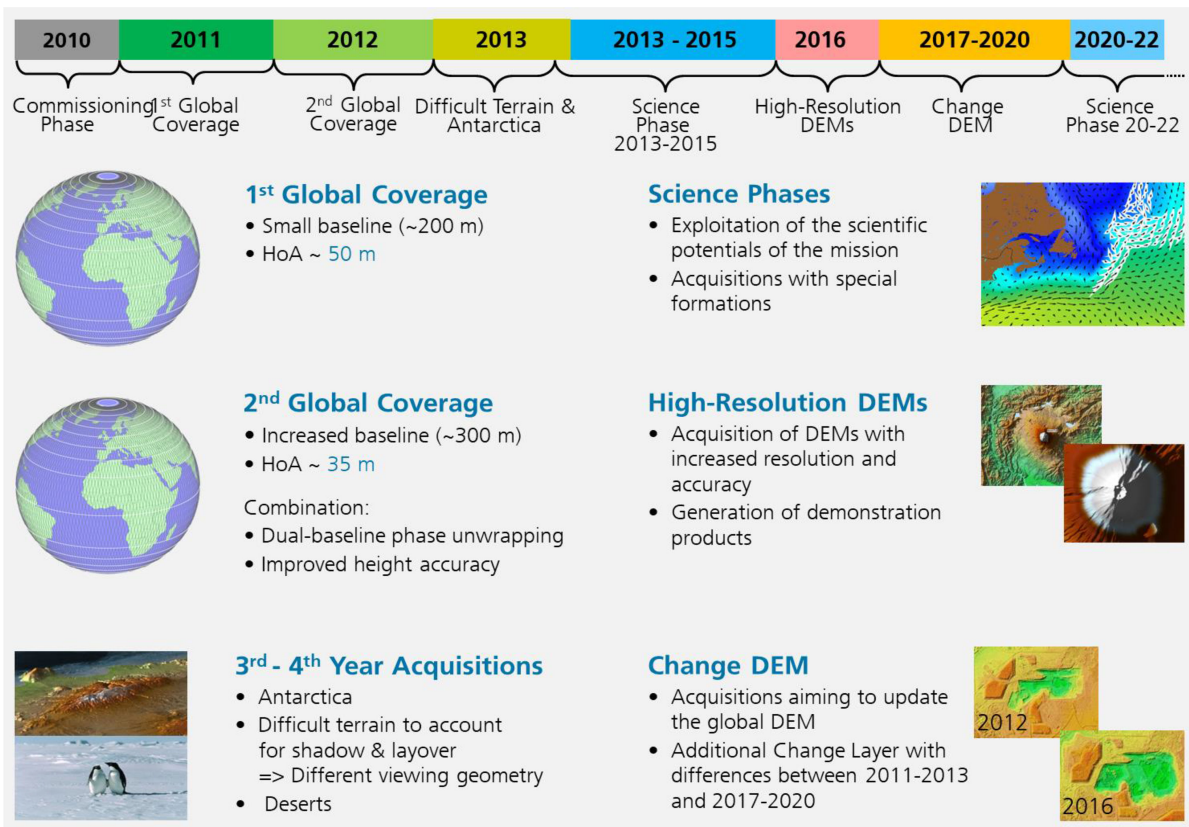


Fig. 5: Mission phases of the TanDEM-X mission.

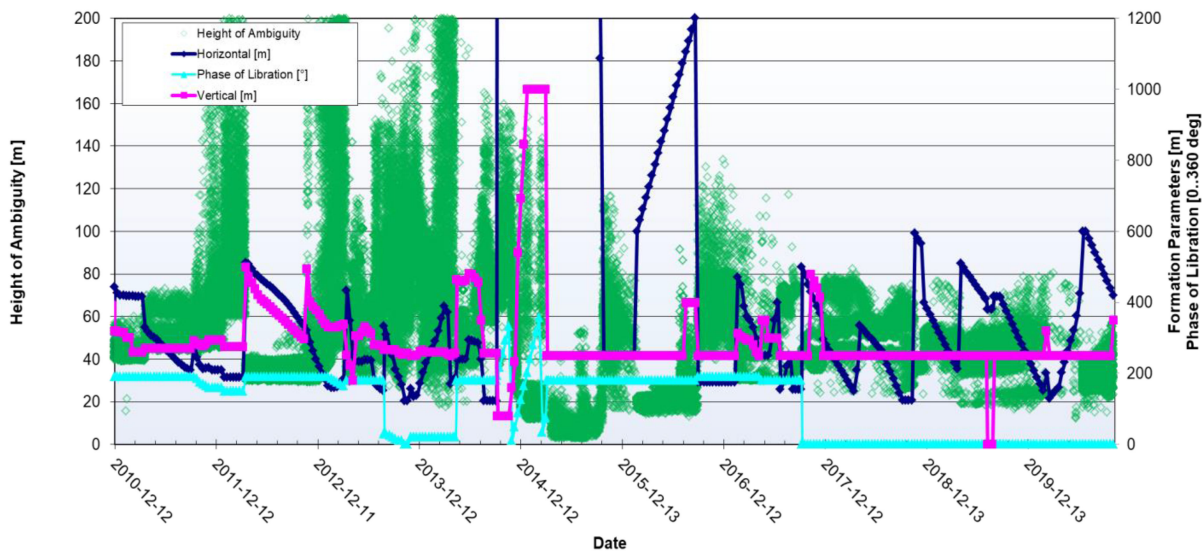


Fig. 6: Evolution of the flight formation parameters over the mission time and corresponding height of ambiguity (green diamonds). The vertical baseline is shown in pink, the horizontal one in blue, and the phase of libration in cyan.

further acquisitions with optimized imaging geometry over critical areas [38], [39]. Referring to the global coherence map derived from the first global acquisition in Fig. 7, one can notice reduced coherence values over forested area, as well as over snow- and ice-covered regions, deserts, and mountainous areas

[40]. Moreover, as described above, dedicated data acquisition strategies have been applied to improve the performance over sandy deserts (by acquiring data with steeper incidence angles, see Fig. 4) and over mountainous regions (with complementary acquisitions from ascending and descending orbits) [41].

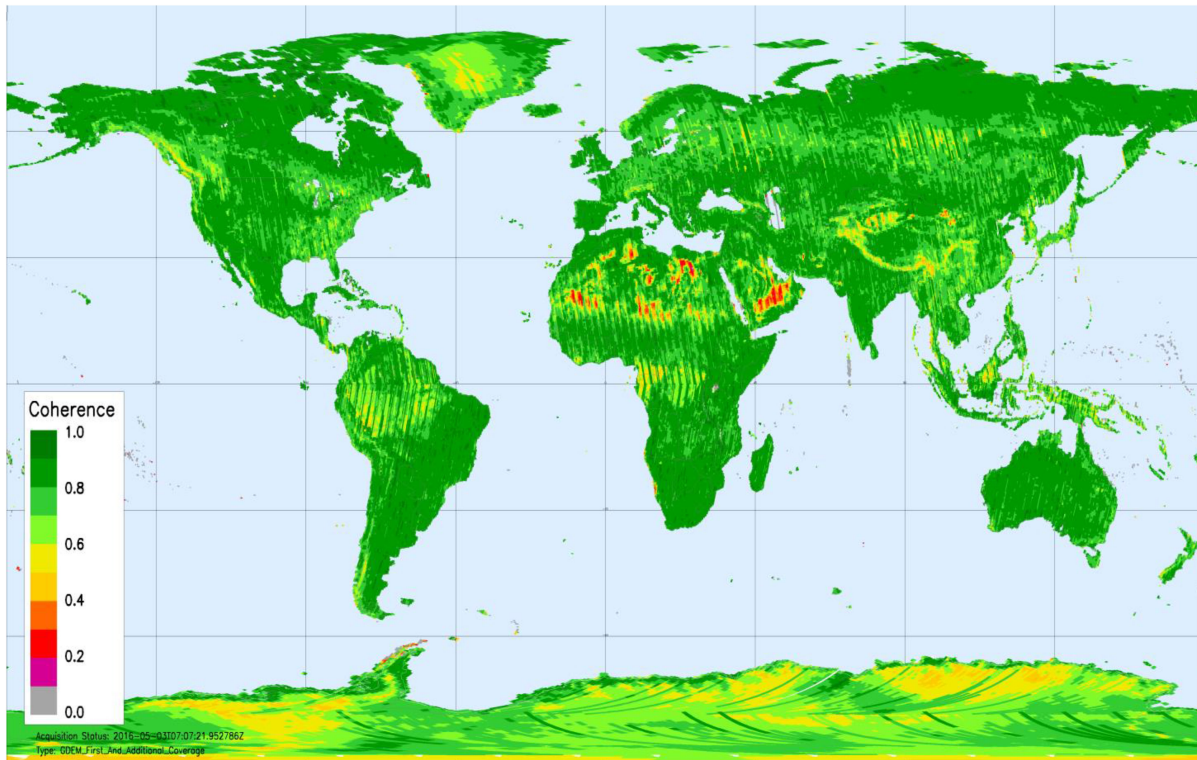


Fig. 7. Global interferometric coherence estimated from the acquisitions of the first TanDEM-X coverage. A coherence of at least 0.6 is required for satisfactory DEM quality.

To complete the global DEM generation, Antarctica has also been acquired twice: during the austral winter - between May and July 2013—and again during the same months in 2014 [41]. This made it possible to achieve a stable performance, as no significant snow melt occurred. The central part of Antarctica (over a radius of 1300 km from the South Pole) cannot be seen in the nominal right-looking imaging mode due to the retrograde polar orbits of TerraSAR-X and TanDEM-X. For this reason, left-looking observations using shallower incidence angles above 50° were required [42].

After completing the acquisitions for the global DEM and a science phase dedicated to experiments with large baselines and polarimetry, bistatic operations continued with high-resolution DEMs and from 2017 to 2020 with the acquisition of data for a global change layer. The next years are dedicated to the frequent monitoring of focus areas.

IV. CALIBRATION OF THE BISTATIC INTERFEROMETER

Data takes for the global DEM are collected in Stripmap mode with a swath width of 30 km. In a fully automated first processing step (see Section V-A), the data takes are divided into individual scenes, so-called Raw DEMs, with an extent of 30 km in range \times 50 km in azimuth. Each Raw DEM already needs to be as close as possible to its real height to allow for an accurate geocoding [43] and to facilitate the second processing step (see Section V-B) in which blocks of the different scenes are calibrated against their neighbors and against ICESat [44] reference heights. The aim

is to further improve their absolute height accuracy and to allow for a seamless mosaicking of adjacent scenes without tilts or displacements.

This section describes the calibration of the bistatic SAR interferometer in order to deliver precise and well-geocoded Raw DEMs. The final DEM calibration is explained in Section V-B.

The interferometric calibration includes three different parts: the calibration of the baseline between both satellites, the adjustment of instrument internal delays to allow for a radar-grammetric determination of the coarse absolute height of the Raw DEM, i.e., to estimate the absolute phase offset, and finally the correction of phase offsets to tune the precise absolute height location of the DEM in the order of a few meters.

Precise baseline determination is performed by a double differential evaluation of GPS carrier phase measurements [45]–[47]. However, primarily due to uncompensated offsets from the SAR antenna phase centers, the relative satellite positions derived from GPS measurements are biased. The accuracy with which the baseline needs to be known is in the order of 1 mm, which corresponds to a height error of roughly 1 m for a typical height of ambiguity of 35 m [3]. For performing the baseline calibration, globally distributed flat test sites with known height are repeatedly acquired. By this, initial offsets in the baseline estimation can be derived and corrected and a monitoring of the baseline stability is subsequently established. The measurements show a standard deviation of 1.31 mm [48], [49]. The remaining

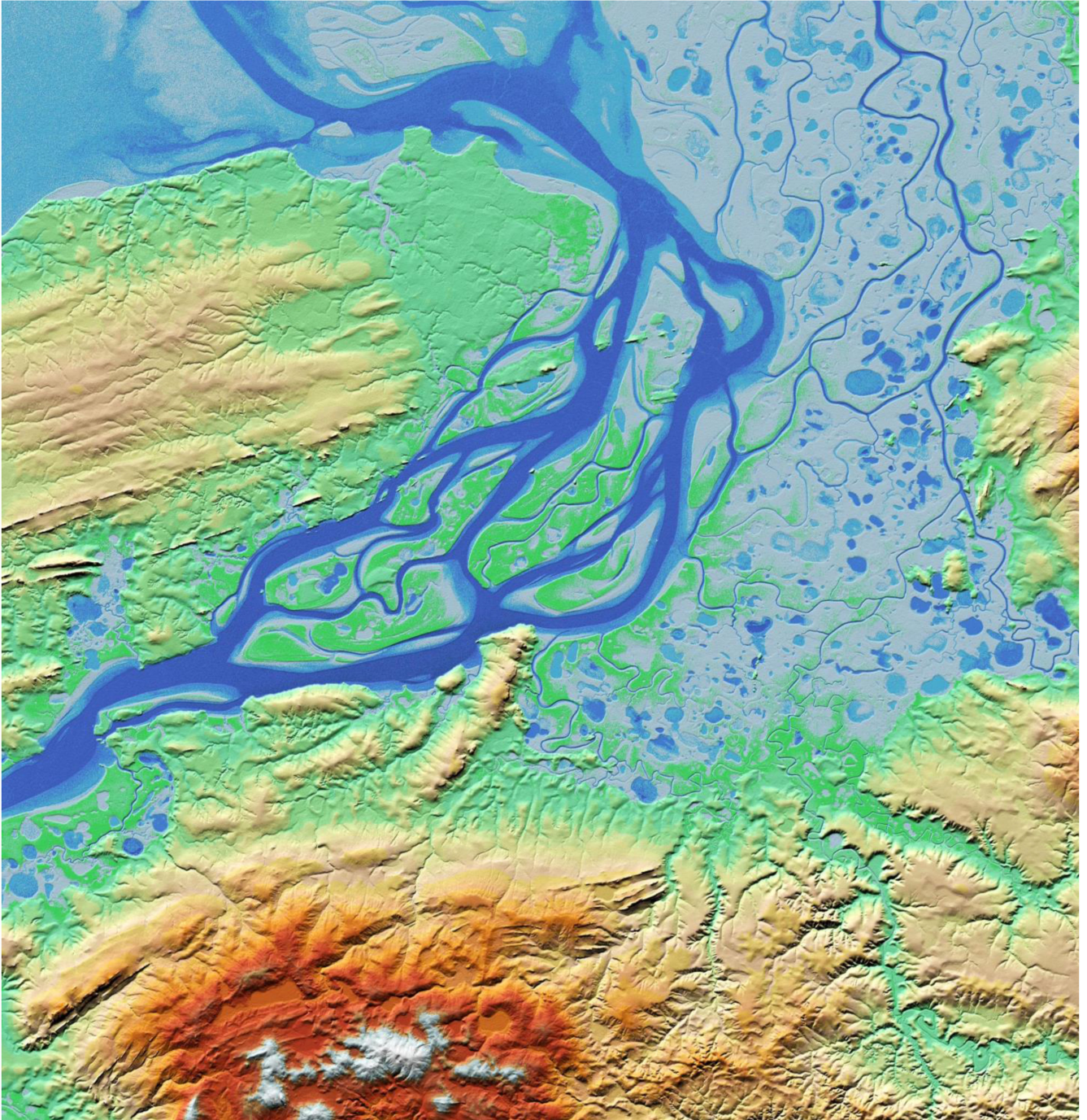


Fig. 8. TanDEM-X DEM covering the area between 73° and 74° North and 86° and 88° East in Russia. The completely frozen river Pjasina meanders into the Kara Sea. The height in this scene varies between 0 m and 280 m.

offsets are applied to the calibrated baseline, which is used for Raw DEM processing.

The interferometric measurement utilizes the phase difference of the acquired SAR data between both satellites. This phase is ambiguous by the wavelength, and thus the correct ambiguity band needs to be resolved. This can be achieved by radargrammetric height determination, which exploits the unambiguous radar signal travel times. For this, a highly precise delay calibration is required to compensate different time delays

in the instruments that can vary depending on radar parameters. Detailed investigations revealed that the delays change with the used synchronization horn antenna, the receiver gain setting, the employed bandwidth, the transmitting satellite, and the position in the orbit [49]. After the determination of appropriate calibration parameters, a correction of the delays is performed in the interferometric processor (see Section V-A).

The final adjustment is performed by calibrating the phase offset between both acquisitions based on a comparison with

reference data (SRTM [1] and ICESat [44]).¹ This phase offset depends on the transmitting satellite, on precise synchronization and start–stop time determination, and on the inclusion of tropospheric path delays [50], [51]. Finally, it has been adjusted such that 90% of all Raw DEMs initially are within ± 10 m versus SRTM/ICESat. The residual 10% are mainly caused by an unresolvable ambiguity in the synchronization link (the so-called π -ambiguity). These ambiguities are largely resolved by reprocessing with a measured phase cycle offset as input which is compensated for in the phase-to-height conversion.

V. DEM PROCESSING CHAIN

The processing from instrument raw data to the final DEM products is performed by two subsequent processors: the Integrated TanDEM-X Processor (ITP) [52] and the Mosaicking and Calibration Processor (MCP) [53].

A. Integrated TanDEM-X Processor (ITP)

The ITP is a systematic and mainly data driven automatic chain which comprises scene-based SAR and interferometric processing. It ingests and screens the incoming acquisitions, focuses the individual scenes in parallel to resampled complex images, calculates the filtered interferogram, performs the phase unwrapping and height precalibration for accurate phase-to-height conversion, and finally generates the geocoded Raw DEMs (see example in Fig. 8). These Raw DEMs are archived along with the associated height error maps, derived from the interferometric coherence, the amplitudes, flag masks, and additional quality control and system calibration data [54].

There are the following four key aspects of the ITP processing chain.

- 1) Synchronization of the instrument phases and bistatic focusing of a highly dynamic satellite formation. Depending on the individual signal travel times, each radar pulse, received at a given time and location by one of the instruments, originates from a different position in space of the transmitting instrument along its orbit. That precise geometric calculation is performed on dense grids and includes the use of a (coarse) DEM of the observed scene as well as the compensation of atmospheric signal propagation effects, as inherited from the TerraSAR-X Multi-Mode SAR Processor (TMSP) [54]–[56]. The formation dynamics require even relativistic corrections of the synchronization signals exchanged between the two satellites [51].
- 2) The next main step is the co-registration, based on coherent cross correlations, and the evaluation of the measured image range shifts as radargrammetric height estimates [43], [57]. The shifts to be applied in resampling of the passive channel are determined in an adaptive approach on small patches. These measurements are accurate enough to derive an absolute height estimate based on the (space and

time-varying) bistatic geometry and a coarsely resolved absolute radargrammetric DEM. The radargram is used throughout the processing chain in combination with the unwrapped interferometric phase to determine an absolute phase offset ambiguity cycle and to estimate and correct larger phase unwrapping errors. Based on the calibration and on such an approach, most of the Raw DEMs are already calibrated to absolute height errors far better than the 10 m required for the final product, independently from any external reference data.

- 3) Following a harmonized acquisition and processing sequence, the landmass is covered at least twice to support the dual-baseline phase unwrapping approach developed for this mission [58], [59]. With smaller height of ambiguity (h_{amb}) values, required to achieve low relative height errors, phase unwrapping is prone to errors. Hence, the data from the more demanding second global coverage are processed with the help of supporting co-registered single-look slant-range complex products from the already processed first coverage. One of the many operational challenges and a limitation of the algorithm is the identification of consistently coherent areas in both acquisitions. Temporal changes (flooding, ice and snow cover, different forest heights, etc.) may inhibit a correction on local scales, while coherent data with suitable height of ambiguity ratios are free from larger errors in 97% of the cases after correction [24], [25].
- 4) Finally, the phase-to-height conversion and Raw DEM geocoding step uses the absolute phase offset from radargrammetry and exactly the same dynamic geometry for the (locally varying) effective baseline as the focusing. Furthermore, atmospheric propagation effects are taken into account based on the same models as established in the TMSP. Additionally, to the monostatic delay, which causes an altitude dependent offset corresponding to spatially varying location and height errors of typically 2–4 m [60], the differential tropospheric phase screen has to be considered as well. A few millimeters of differential propagation delay from slightly different viewing angles cause height offsets of up to 3 m if not properly compensated [61].

B. Mosaicking and Calibration Processor (MCP)

After Raw DEM generation, the last two steps for the production of TanDEM-X DEM products consist of 1) the calibration of DEM acquisitions to reference and tie point heights (DEM calibration) and 2) the mosaicking of single interferometric Raw DEMs (DEM mosaicking).

DEM calibration requires a global set of suitable height references. For TanDEM-X, the ICESat data are used as ground control points (GCP). The ICESat spaceborne laser altimeter provides precise height references at a sampling distance of 170 m in along-track and a maximum across-track distance of 80 km at the Equator [44]. A small subset of selected (no vegetation and mostly flat areas) ICESat points is used for calibration, and a much higher number is used later on for validation of the final DEM heights [62]. Second, tie points in the

¹SRTM is used for absolute height comparison in the latitude regions between $\pm 60^\circ$. ICESat points are used for regions outside the SRTM coverage.

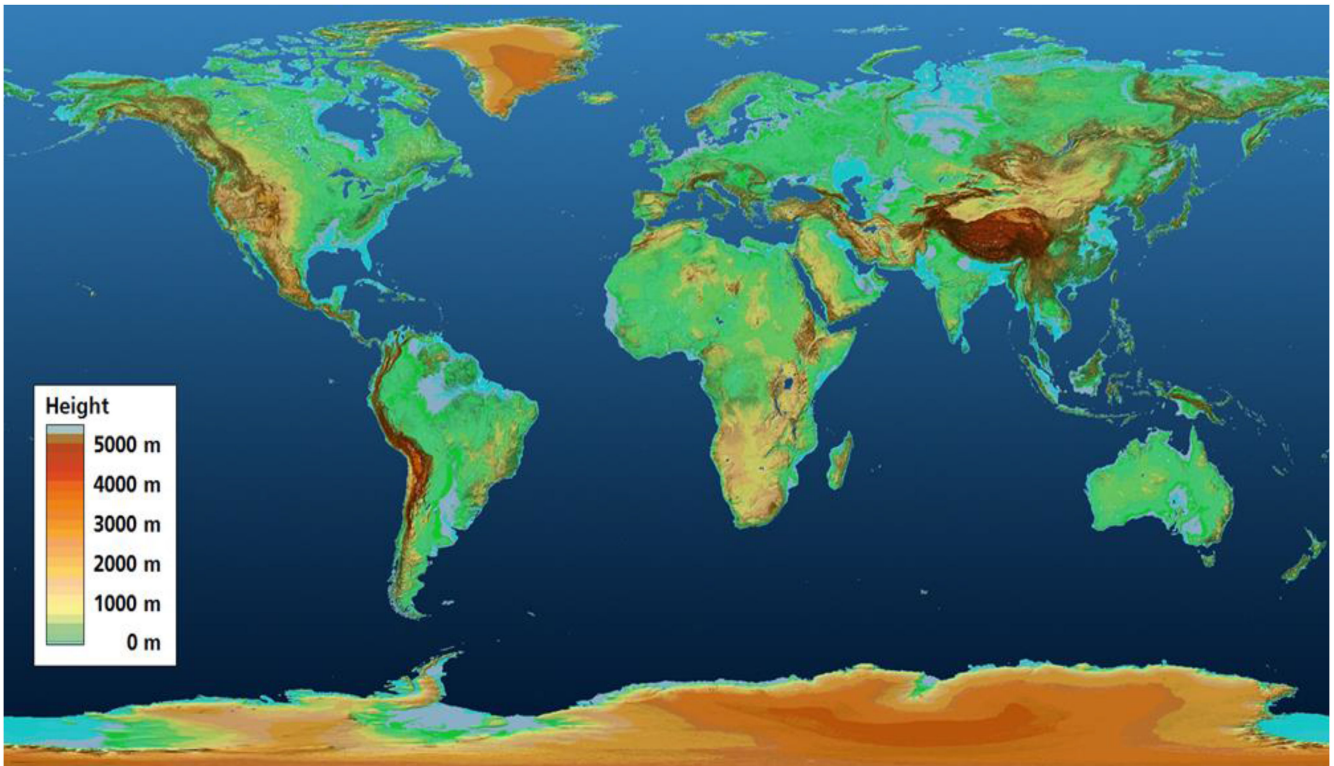


Fig. 9. Global TanDEM-X DEM is a consistent data set covering all land surfaces at a posting of $12\text{ m} \times 12\text{ m}$ and at an unprecedented absolute height accuracy of about 1 m for bare surfaces and 3.5 m overall (see Table II). Data coverage is close to 99.9% of the total land surface area.

more than 3 km wide overlap between neighboring DEM swaths are used to ensure the relative height calibration. Estimates for each data take offset, tilt in range, and slope in the azimuth direction are derived by means of a weighted least-squares adjustment [63].

In the mosaicking, the calibration corrections are applied to each DEM and different coverages are mosaicked by a weighted average of the elevation values, where the weights are derived from the relative height errors. Relative height error values are also fused together with the help of the relative height error map (HEM) [64].

As X-band radar waves are able to penetrate in snow and ice by several meters, special adaptations to the nominal DEM calibration are necessary to provide the X-band reflective surface. The outer coastal regions of Greenland are mostly characterized by steeper bare areas, where the radar height matches quite well with the one retrieved from ICESat. Thus, the block adjustment solely relies on GCPs at the coastal rim of Greenland [65]. Antarctica is too large and there are not enough bare surfaces. Therefore, areas characterized by homogeneous backscattering characteristics and hence predominantly homogeneous penetration depths are chosen. For each of these areas, the mean height difference between the TanDEM-X and ICESat elevation information is calculated. Contrary to all other landmasses, for Antarctica this height difference is not removed but rather used as a constant bias in the mosaicking, referring the entire block to a mean InSAR height (i.e., phase center at X-band) below the surface. Starting from these fixed blocks, all other

Antarctica acquisitions are adjusted solely relying on tie points and on the already calibrated areas, as for the Greenland's inner areas.

VI. GLOBAL DEM PERFORMANCE

The global TanDEM-X DEM (see Fig. 9) is partitioned into more than 19 000 so-called geocells covering $1^\circ \times 1^\circ$ in latitude and longitude [64], [65]. Each geocell product contains the DEM as well as various layers that provide the user with additional information, such as the HEM, the mosaic of the mean amplitude (AMP), a water indication mask (WAM), and a coverage mask (COV). Beyond the full resolution version sampled at 12 m (0.4 arc second), reduced resolutions multilooked at 30 m (1 arc second) and 90 m (3 arc second) posting are also available [65].

The performance presented in this section is assessed separately for three different classes of DEM geocells according to the dominant land cover type: forest geocells, characterized by more than 60% of forest coverage; ice geocells, with more than 60% of ice or snow coverage; and generic geocells, i.e., all other geocells [66]. As described in Section III, the first two types are strongly affected by volume decorrelation [67].

A. Absolute Height Accuracy

The absolute vertical accuracy represents the uncertainty in the height of a point with respect to the WGS84 ellipsoid caused by uncorrected, slow-changing systematic errors. The evaluation of the final TanDEM-X DEM performance is based on the

TABLE II
SUMMARY OF THE ABSOLUTE HEIGHT ACCURACY, EVALUATED USING THE BEST (FLATTEST FOOTPRINT) 1000 ICESat VALIDATION POINTS PER DEM GEOCELL [66]

Statistics	Generic geocells	Ice geocells	Forest geocells	All geocells
Number of geocells	12,257	3,019	4,113	19,389
Landmass [million km ²]	96.68	14.31	33.22	144.21
Accumulated number of validation points (millions)	10.20	2.71	2.58	15.49
Mean height deviation of validation points [m]	0.04	-2.83	0.57	-0.37
Accumulated absolute height accuracy of 10 m (linear error)	99.84%	98.42%	99.17%	99.48%
Accumulated absolute height accuracy with 90% linear error [m]	0.88	6.37	2.33	3.49

difference between TanDEM-X and ICESat points not used in the DEM calibration. On a global scale, the performance in terms of absolute vertical accuracy has been evaluated using the best 1000 ICESat validation points per DEM geocell, characterized by the lowest spatial variance, and thus tending toward moderate-relief terrain. The prioritization of flat regions in the evaluation does not compromise the validity of the proposed method, as the main error sources are the remaining tilts and low-varying trends, which affect the entire geocell. The results confirm the outstanding capabilities of the system, with an overall absolute height accuracy at a 90% confidence level of just 3.49 m, which is well below the 10 m mission specification [66], [68] (see Table II). Excluding highly vegetated and snow/ice-covered regions characterized by radar wave penetration phenomena and consequently strongly affected by volume decorrelation, the absolute height accuracy improves to 0.88 m (for generic geocells only). The geocell-based absolute height accuracy at 90% confidence level is depicted in Fig. 10 (top). The effects of penetration are clearly visible over ice-covered and forested areas, where offsets between TanDEM-X and ICESat in the order of several meters are detected.

B. Relative Height Accuracy

The relative height accuracy - or point-to-point vertical accuracy—describes the precision of the local height differences and only accounts for random errors [69]. The relative height accuracy for each input observation can be directly estimated from the interferometric coherence and the number of looks by assuming a zero-mean Gaussian distribution [70]. For each geocell of the mosaicked TanDEM-X DEM, the estimation of the linear point-to-point confidence level for the specified height accuracy is derived from the HEM - separately for flat (predominant slope lower than 20%) and steep terrain (predominant slope higher than 20%) [71], [72].

An overview of the relative height accuracy of the final TanDEM-X DEM per geocell is shown in Fig. 10 (bottom). Geocells in dark green and turquoise have an estimated confidence level below 90% and are either dominated by forest or mostly covered by snow or ice. Such geocells are affected by volume decorrelation phenomena, which artificially degrade the interferometric coherence. For this reason, they are excluded from the validation process. The same exclusion applies to

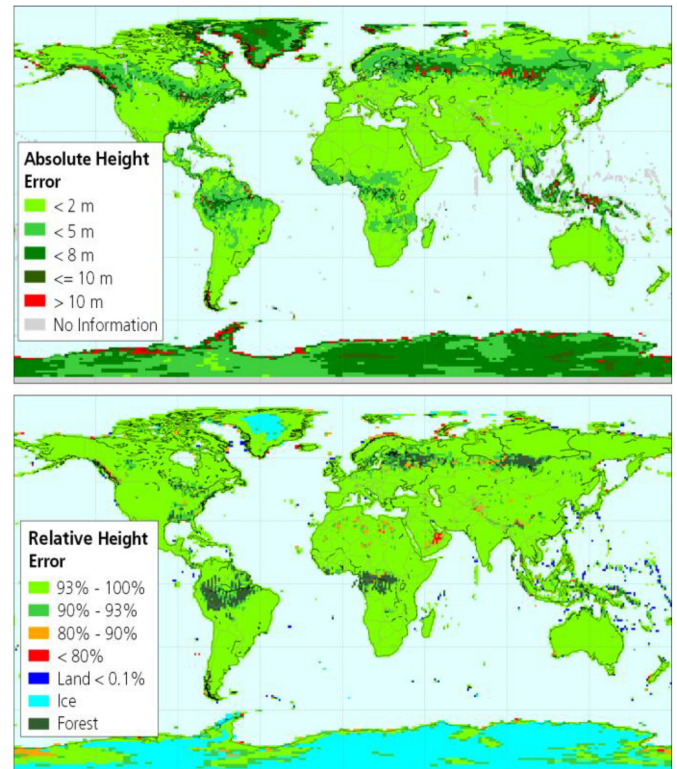


Fig. 10. Geocell-based global DEM performance in terms of absolute height accuracy (top) and relative height accuracy (bottom).

geocells dominated by water bodies (i.e., cells with land fraction below 0.1%, depicted in blue). The mission specification at 90% confidence level (2 and 4 m for flat and steep terrain, respectively) is met on a global scale for 97.76% of all geocells not excluded due to volume decorrelation effects [73].

C. Voids

Of the total TanDEM-X dataset, voids over land account for only 0.107% of the entire Earth's landmass or, in other words, the data coverage is better than 99.89% [74].

Besides the global validation, several additional quality analyses have been performed using local reference datasets, such as kinematic GPS tracks [75], lidar, and other global DEM data

TABLE III
SUMMARY OF THE ABSOLUTE HEIGHT ACCURACY, EVALUATED USING
KINEMATIC GPS VALIDATION POINTS

Statistics	
Total length of tracks [km]	66,262
Number of GPS points (millions)	3.12
Mean height error [m]	-0.17
Standard deviation [m]	1.28
absolute height accuracy with 90% linear error [m]	1.93

[76], [77]. The results (see, e.g., Table III) are well in line with the numbers reported above and confirmed the high accuracy of the height data.

The generation of the global DEM, which is the primary mission objective, was successfully completed in September 2016. DEM performance specifications have all been met or exceeded [78], [79]. In the case of the absolute height accuracy, the final result is one order of magnitude better than the 10 m requirement, as summarized in Table II. A world-wide, consistent and up-to-date DEM of that quality is of fundamental importance for a wide range of scientific and commercial applications. The edited version of the TanDEM-X DEMs are among the few remote sensing datasets that are commercially viable [80] and have been supplied to the ESA/EC Copernicus Programme, i.e., the so-called Copernicus DEM [81] is basically an edited version of the TanDEM-X Global DEM and is free and open at a posting of 30 and 90 m. The scientific community is being served by DLR providing access even to the full resolution 12 m DEMs at no costs via a standard Announcement of Opportunity process, see Section IX. Currently more than 4000 scientists from 97 countries are registered on the TanDEM-X science server.

VII. FURTHER GLOBAL PRODUCTS

Multiple global coverages have been acquired for the generation of the global DEM. These unique interferometric data sets contain much more than the surface topography and allow for the derivation of additional global layers like the global TanDEM-X Forest/Non-Forest map. Furthermore, an edited version of the DEM and, as a by-product, a global water body layer are being generated.

A. Global TanDEM-X Forest/Non-Forest Map

The global coherence data that have been primarily used to monitor and control the data acquisition contain interesting information on the surface cover that can be used to discriminate vegetated from non-vegetated areas and to derive a global TanDEM-X Forest/Non-Forest Map [82]. The used dataset comprises all TanDEM-X images acquired for the generation of the global DEM between 2011 and 2015. To limit the computational load, quicklook data (with a spatial resolution of 50×50 m) of the bistatic coherence and the information on the acquisition geometry have been used. The amount of volume decorrelation can be directly derived from the interferometric coherence

and has been used as main indicator for the identification of vegetated areas in a machine learning classification method based on a supervised fuzzy clustering, specifically trained for different kinds of forests. For each pixel on the ground, all available independent observations are then combined by taking into account the reliability of each input measurement. Other information available at scene level, such as layover and shadow layers, the local incidence angle, and the height of ambiguity, are also exploited in the mosaicking process. Finally, additional annotation layers are utilized or directly generated to filter out water bodies, cities, deserts, and geographic regions above the altitude of the tree line, where no tall vegetation can grow. For this purpose, a global map of the tree line boundary altitude has been derived by combining information from the TanDEM-X global DEM and the GlobCover classification map provided by the European Space Agency [84]. The global TanDEM-X Forest/Non-Forest map is presented in Fig. 11. It was validated against external high-resolution reference information as well as other classification maps and an overall agreement often exceeding 90% was observed [82].

B. Global Urban Footprint

The Global Urban Footprint is a binary layer which identifies urban settlements world-wide. The product has been derived by applying an automated classification procedure to full-resolution amplitude images acquired by the TerraSAR-X and TanDEM-X satellites for the generation of the global DEM [83].

C. Water Body Layer

The TanDEM-X Water Body Layer (WBL) is a new global product derived from bistatic InSAR data. Low values of coherence are indeed a good indicator of the presence of water on ground and are therefore used as input for a single-scene classifier based on the watershed segmentation algorithm. As for the Forest/Non-Forest Map, quicklook images at 50×50 m resolution, acquired between 2011 and 2015, are used in order to limit the computational burden. Given the high seasonal variability of water levels as well as changes in river beds, it is possible to keep track of such changes by exploiting the multitemporal information from subsequent global coverages. This allows for the discrimination between permanent and temporary water, depending on the occurrence of water detection in overlapping acquisitions. An example of the Amazon River over the State of Pará, Brazil, is presented in Fig. 12. The global TanDEM-X WBL product will be finalized in 2021. Preliminary validation activities with respect to both high-resolution layers and global products show a test accuracy measure F-score typically above 90% when the extent of water in the geocell is above 2%.

D. Edited DEM

The delivered global TanDEM-X DEM is an unedited version, i.e., voids over land are not filled and water surfaces appear noisy. Nevertheless, an edited product is required in many different application spheres, spanning from hydrogeological modelling to InSAR processing and geocoding of remote sensing data.

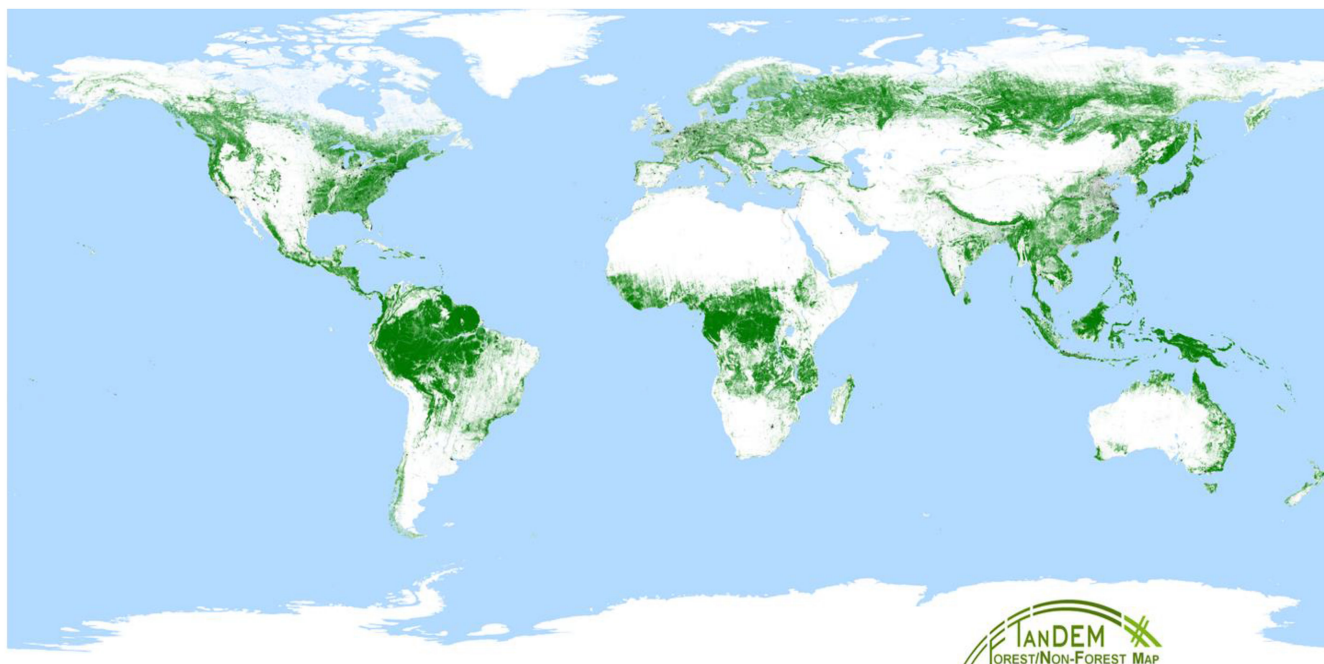


Fig. 11. TanDEM-X Forest/Non-Forest Map (green: forest, white: non-forest, light blue: water).

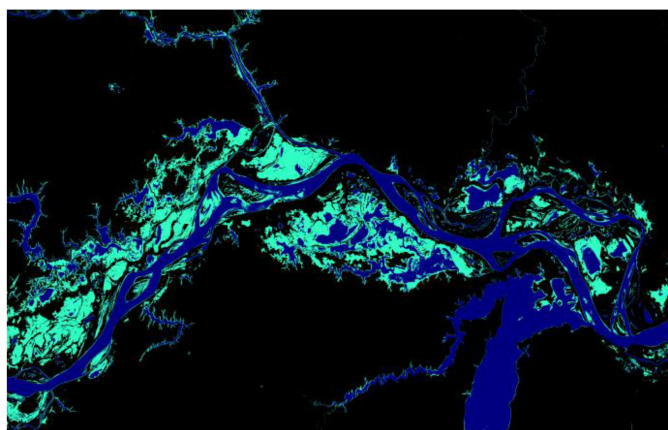


Fig. 12. Detail of the global TanDEM-X Water Body Layer showing the variability of the Amazon River over the State of Par , Brazil. Blue identifies permanent water, while light green corresponds to temporary water.

Up to now, an edited version of the global DEM, the so-called WorldDEM, has been commercialized by Airbus Defence & Space [80].

For noncommercial applications of the TanDEM-X data, a fully automatic procedure for editing the global TanDEM-X DEM has now been developed at DLR as well [85]. It comprises void filling depending on the size of the gaps either through interpolation of neighbor pixels or using external reference DEMs and water flattening. The latter makes use of the TanDEM-X WBL (see Section VII-C) for identifying water surfaces to be properly smoothed. The algorithm is applied to the 30 m DEM version for all landmasses except for Antarctica. An example is

depicted in Fig. 13, where both void filling and water flattening effects are clearly visible.

For Polar Regions a dedicated editing has been implemented [86]. The improvements of the TanDEM-X PolarDEM 90 product comprise gap filling with newer acquisitions, smoothing of noisy areas, interpolation of voids and replacement of frozen and open sea areas with geoidal heights [87]. The Time Tagged TanDEM-X PolarDEM 90 product contains the unedited height for single winter seasons. It will be provided as X-band radar surface and in addition by applying the penetration bias [5] due to volume scattering (see Section III) [88].

E. Change DEM

The global TanDEM-X DEM clearly demonstrated that, given its outstanding accuracy, height differences are visible between interferometric SAR data acquired at different times. As a matter of fact, even small height changes in glaciers, forests but also those caused by agricultural activities or infrastructure changes are well detectable in the X-band DEM. Therefore, in 2017 it was decided to acquire an additional complete coverage of the Earth's landmass. The aim is to provide an independent DEM dataset representing a well-defined time span from September 2017 until mid-2020. This additional dataset will allow for an assessment of topographic changes with respect to the previous TanDEM-X DEM product on a global scale. The new product benefits from the experience gained in the generation of the global the global TanDEM-X DEM. Improvements in both the acquisition planning and the data processing enable reliable DEM generation at high accuracy with fewer acquisitions [89], [90]. To achieve this demanding goal, the use of an edited TanDEM-X DEM as "starting point" for the phase unwrapping

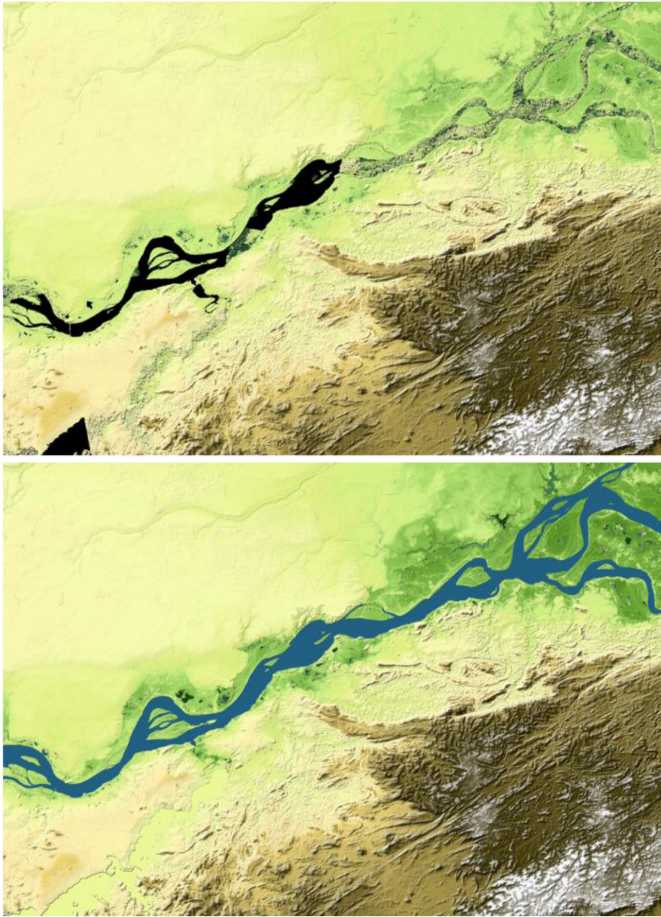


Fig. 13. Example of the automatic editing of the global TanDEM-X DEM. Top: unedited DEM, bottom: edited version after void filling and water flattening.

and calibration is required, allowing for the systematic detection of 3-D temporal changes. To this purpose, the automatically edited global TanDEM-X DEM presented in the previous section is being used, together with the TanDEM-X PolarDEM for Antarctica and Greenland. An example of the height differences of a Change Raw DEM with respect to the edited TanDEM-X DEM is presented in Fig. 14 .

VIII. DEMONSTRATION OF NEW TECHNIQUES AND APPLICATIONS

The scientific exploitation of TanDEM-X goes far beyond the DEM and the unique capabilities enable numerous secondary mission objectives based on along-track interferometry as well as new bistatic and multistatic SAR techniques. Several bistatic experiments were already conducted during the TanDEM-X commissioning phase [91]–[93]. When the geometry was appropriate during the operational DEM phase, additional scientific data takes have been included into the timeline from the very beginning. After completion of the data acquisition for the global DEM, a dedicated science phase was introduced from 2013 to 2015 to exploit the unique features of the TanDEM-X mission. Large cross-track baselines of up to 4 km allowed for the acquisition of high-resolution DEMs and for polarimetric SAR

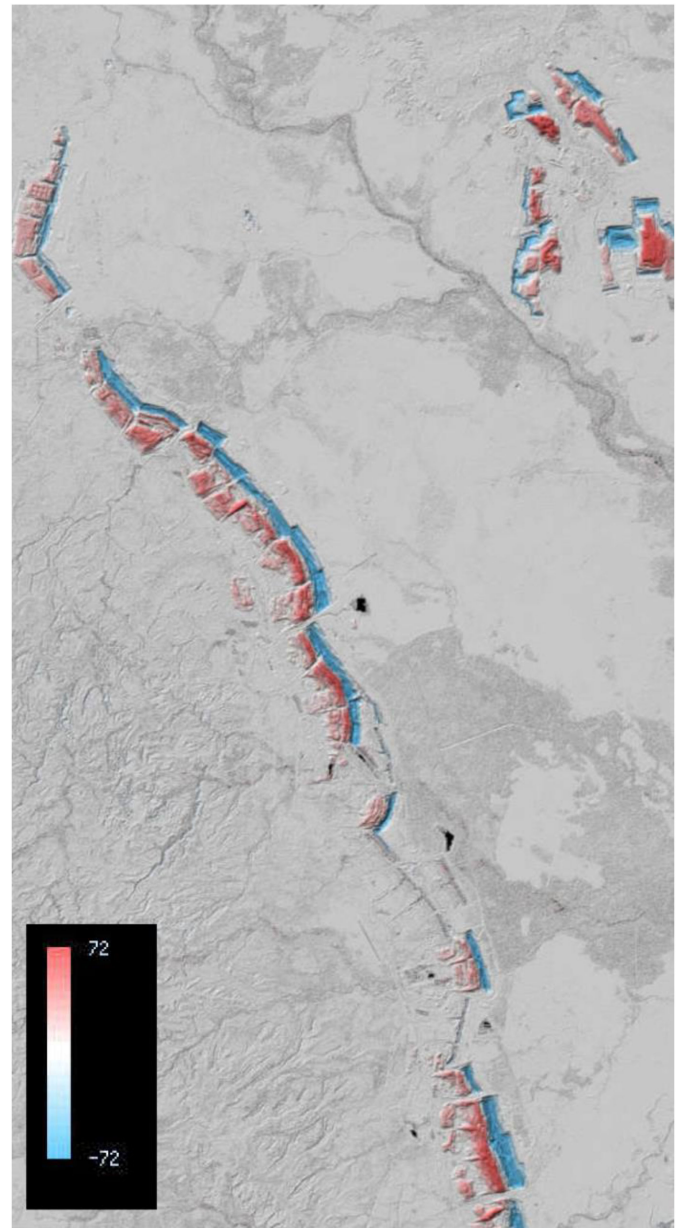


Fig. 14. Example of the height differences with respect to the edited TanDEM-X DEM product for a coal mining area in Queensland, Australia. The color table indicates height changes in meter.

interferometry experiments over agricultural fields. The science phase also included an along-track interferometry campaign, for which suitable baselines have been adjusted over tests on the northern and southern hemisphere. To further improve the control accuracy of the satellite formation along-track, the so-called TanDEM-X Autonomous Formation Flying system has been activated [94]. For a few months the satellite twins flew at an along-track distance of 76 km (corresponding to about 10 s time lag) and operated in the pursuit monostatic mode. After the science phase, close formation flight was re-established in 2016 and has been kept until today. In the last 4 years further experiments and demonstrations have been carried out without

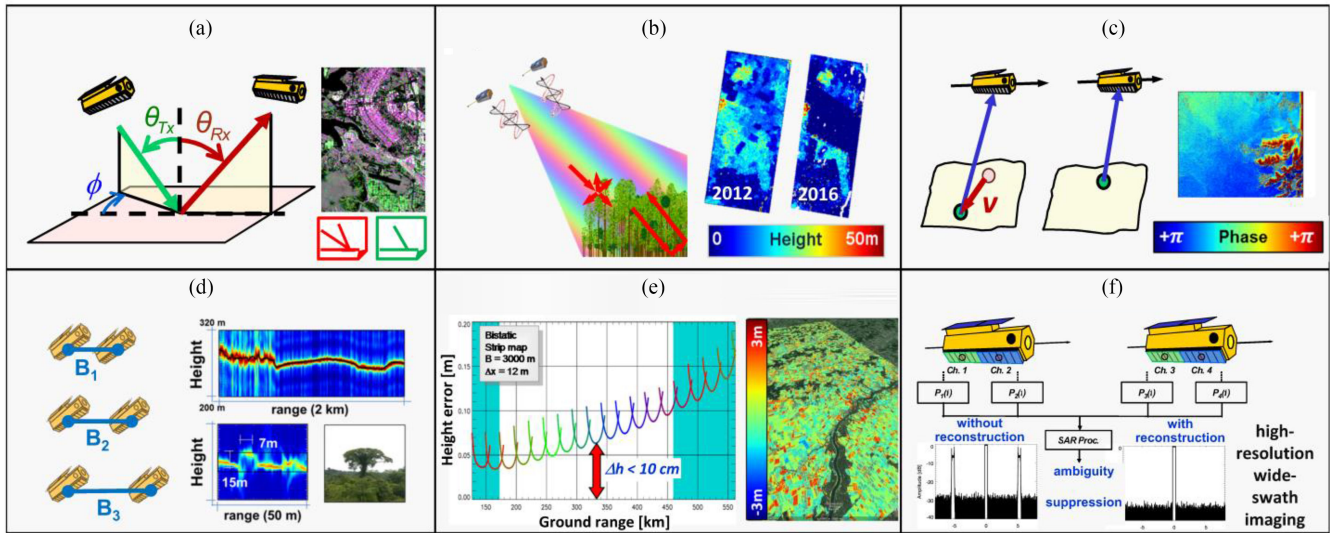


Fig. 15. Examples of demonstration of new techniques with the TanDEM-X mission showing potential applications for future bistatic and multistatic SAR missions. (a) Bistatic SAR imaging [91]–[93]. (b) Polarimetric SAR interferometry [96], [98]. (c) Along-track SAR imaging for ocean current velocity estimation [94], [99]. (d) SAR tomography for tree height estimation [96], [97]. (e) Double differential interferometry for crop height estimation [102]. (f) Digital beamforming with four phase centers for ambiguity suppression [103]–[105].

jeopardizing the operational data acquisition of the TanDEM-X mission.

Among the innumerable demonstrations of new techniques and applications, the following examples summarize the potential of future bistatic and multistatic SAR missions as well as the high flexibility of the ground segment and of the radar instruments of both satellites (see also Fig. 15).

- 1) High-resolution digital elevation model based on multiple single-pass interferometric acquisitions [95].
- 2) Polarimetric SAR interferometry and SAR tomography for tree height estimation [96]–[98].
- 3) Along-track SAR imaging for ocean current velocity estimation [94], [99].
- 4) Bidirectional along-track interferometry for 2-D ocean current velocity estimation [100], [101].
- 5) Double differential interferometry for crop height estimation [102].
- 6) Digital beamforming with four phase centers for ambiguity suppression [103]–[105].
- 7) Pursuit monostatic along-track interferometry for ice floe rotation estimation [106].
- 8) Boreal forest biomass estimation [107].
- 9) Ship velocity and rotation estimation [108].
- 10) Ice sheet penetration depth estimation and ice sheet classification [5].
- 11) Bistatic imaging [92].
- 12) Glacier height change due to ice melting [111].
- 13) Permafrost disturbance and height changes [112].
- 14) Sea ice height estimation [113].
- 15) Two-Look TOPS interferometry for estimation of azimuth displacements [109], [110].

Furthermore, throughout the mission selected, super sites (e.g., outlet glaciers in Antarctica or Greenland) have been regularly observed. Such datasets are usually processed to

co-registered single-look slant-range complex (Co-SSC) products and provided to members of the science team for multitemporal analyses, for example, using such data dramatic ice loss has been reported for outlet glaciers on the polar ice caps [114] as well as inland glaciers [111], [115].

The TanDEM-X Science Team has been instrumental in utilizing, validating, and innovating TanDEM-X DEMs and other products, leading to many new science results and applications. In the last ten years, invited sessions on TanDEM-X at IGARSS and EUSAR conferences have showcased these results.

IX. SCIENCE ACTIVITIES

The coordination of the international science team and the data take planning have been one of the major tasks, and has substantially contributed to the dissemination of the mission data. Since 2010 six special announcements of opportunity (AO) have been launched for data take requests and over 1500 proposals have been received from 1140 science investigators worldwide.

TanDEM-X 12-m DEMs were in high demand by science community members, with approximately 900 proposals and over 17 000 data products (geocells). The top three application spheres are geosphere, cryosphere, and hydrosphere with a regional focus on Europe, Asia, all mountainous areas and the polar regions (Greenland and Antarctica). Proposal submissions are accepted at any time through the general announcement of opportunity.² The 90 m DEM product is available to the science community without the need to submit a proposal. Upon simple registration, it is possible to download the data globally via an FTP server.³ Dedicated future AOs are planned for the exploitation of the 30 m DEM and the Change DEM.

²Online. [Available]: <https://tandemx-science.dlr.de/>

³Online. [Available]: <https://download.geoservice.dlr.de/TDM90/>

One additional task for the science coordination is to foster the exchange and feedback from the scientists that have used the data. The scientific results of the principal investigators have been presented in regular coordinated sessions at several international conferences (EUSAR 2012–2021 and IGARSS 2011–2020) and the bi-/tri-annually organized TanDEM-X science team meetings at DLR in Oberpfaffenhofen, Germany. Approximately 200 to 300 scientists have presented their results in oral or poster presentations at the science team meetings, held every two or three years from 2006 to 2019.

X. CONCLUSION AND OUTLOOK

At its inception, the TanDEM-X mission was conceived as a first-of-a-kind system to produce the world's most accurate global topographic dataset, and to do so by employing key new technologies such as close formation flying, bistatic SAR operation and synchronization, precise baseline estimation and calibration, as well as sophisticated bistatic and interferometric processing and calibration chains. After ten years of successful operation, it remains unique worldwide and continues to provide new insights into our changing Earth, and new ideas for radar remote sensing techniques and phenomenological investigation. It is this combination of technology driver and excellent quality of mission products that makes TanDEM-X unique and a milestone for future developments.

Accurate topographic information is a fundamental layer for essentially all Earth science disciplines. SRTM has been the topographic standard for the last 20 years and has been continuously and repeatedly downloaded. SRTM was also the forerunner of TanDEM-X, that was designed to generate a next higher-level of DEM quality. This objective has been achieved with the global TanDEM-X DEM being well within specification; the achieved absolute height accuracy exceeds the 10 m specification by almost one order of magnitude and the coverage is close to 99.9%. In the version of the Copernicus DEM, TanDEM-X fulfills all prerequisites to become the new topographic standard, thus advancing the success story of its predecessor SRTM.

It is expected, that formation flying bistatic and multistatic interferometry will become a standard technique in radar remote sensing as it allows not only the generation of precise DEMs, but also enables SAR tomography for observation of the 3-D structure of volume scatterers. Tandem-L [116], a proposal for an environment and climate monitoring mission and for capturing dynamic processes on the Earth surface, builds in large parts on TanDEM-X. As a bistatic L-band system it enables tomographic observations of forest and the derivation of the 3-D structure as a prerequisite for a precise determination of the global biomass and its changes, a central and so far, only insufficiently known quantity in the carbon cycle. Currently, efforts are underway to implement such a bistatic L-band mission within the framework of ROSE-L in the European Copernicus program [117].

TanDEM-X was also used to demonstrate new bistatic and multistatic SAR techniques, that are of great importance for future distributed SAR missions based on formation flying [118], [119]. A first example is Germany's follow-on X-band mission

high-resolution wide-swath (HRWS) [120], which consists of a high-resolution main satellite with multiple azimuth aperture phase centers and a frequency scanning functionality in elevation taking advantage of the high system bandwidth (1200 MHz). In response to strong user requirements for single-pass interferometry and 3-D imaging, the so-called MirrorSAR concept has been developed [121]. MirrorSAR consists of three low-cost receive-only companion satellites, that fly on different Helix orbits about 15 km ahead of the main satellite. The receiver satellites are considerably simplified, as their main functionality is reduced to a kind of microwave mirror (or space transponder) which routes the radar echoes toward the transmitter. This multistatic approach enables simultaneous acquisitions in three baselines for robust single-pass interferometry and generation of DEMs at 4 m posting and relative height accuracies similar to TanDEM-X. Funding for HRWS has been recently approved by the German government with a launch foreseen for end 2026.

Both TSX and TDX have by far exceeded the nominal lifetime of 5.5 years. The quality of the global DEM generated by TanDEM-X is unsurpassed and allows detecting height changes down to the meter range. Therefore, data for a global TanDEM-X DEM version 2.0 or Change DEM have been acquired in the last years. First results show a highly dynamic Earth surface with, e.g., melting glaciers and ice sheets, deforestation in tropical forests or mining activities. Capturing these dynamic processes was not originally planned, but further increases the value of the TanDEM-X mission with increasing lifetime. Predictions on the current status of system resources indicate up to five more years (until 2025) of operation. In the coming years, the focus will be on global 3-D observations of the cryosphere, forests, and large cities with a short revisit.

ACKNOWLEDGMENT

The authors would like to thank the anonymous reviewers for their valuable comments and suggestions that helped to improve this article. They would also like to acknowledge the extraordinary effort of all colleagues at DLR, Airbus Defence & Space, and the Helmholtz Centre Potsdam (GFZ) for making this ambitious idea a reality and a great success.

REFERENCES

- [1] T. G. Farr *et al.*, "The shuttle radar topography mission," *Rev. Geophys.*, vol. 45, no. 2, 2007, Art. no. RG2004.
- [2] A. Freeman, M. Zink, E. Caro, A. Moreira, L. Veilleux, and M. Werner, "The legacy of the SIR-C/X-SAR radar system: 25 years on," *Remote Sens. Environ.*, vol. 231, 2020, Art. no. 111255.
- [3] G. Krieger *et al.*, "TanDEM-X: A satellite formation for high resolution SAR interferometry," *IEEE Trans. Geosci. Remote Sens.*, vol. 45, no. 11, pp. 3317–3341, Nov. 2007.
- [4] A. Moreira *et al.*, "TanDEM-X: A TerraSAR-X add-on satellite for single-pass SAR interferometry," in *Proc. Int. Geosci. Remote Sens. Symp.*, Anchorage, USA, 2004, vol. 2, pp. 1000–1003.
- [5] P. Rizzoli, M. Martone, H. Rott, and A. Moreira, "Characterization of snow facies on the Greenland Ice Sheet observed by TanDEM X interferometric SAR data," *Remote Sens.*, vol. 9, no. 4, 2017, Art. no. 315.
- [6] R. Werninghaus and S. Buckreuss, "The TerraSAR-X mission and system design," *IEEE Trans. Geosci. Remote Sens.*, vol. 48, no. 2, pp. 606–614, Feb. 2010.
- [7] W. Pitz and D. Miller, "The TerraSAR-X satellite," *IEEE Trans. Geosci. Remote Sens.*, vol. 48, no. 2, pp. 615–622, 2010.

- [8] O. Montenbruck, R. Kahle, S. D'Amico, J.-S. Ardaens, "Navigation and control of the TanDEM-X formation," *J. Astronautical Sci.*, vol. 56, no. 3, pp. 341–357, 2008.
- [9] R. Kahle, B. Schlepp, F. Meissner, M. Kirschner, and R. Kiehling, "The TerraSAR-X /TanDEM-X formation acquisition – From planning to realization," *J. Astronautical Sci.*, vol. 59, pp. 564–584, 2012.
- [10] E. Maurer, R. Kahle, G. Morfill, B. Schlepp, and S. Zimmermann, "Reversal of TanDEM-X's relative motion from counter-clockwise to clockwise," *SpaceOps*, 2014.
- [11] G. Krieger and M. Younis, "Impact of oscillator noise in bistatic and multistatic SAR," *IEEE Geosci. Remote Sens. Lett.*, vol. 3, no. 3, pp. 424–428, Jul. 2006.
- [12] M. Younis, R. Metzger, and G. Krieger, "Performance prediction of a phase synchronization link for bistatic SAR," *IEEE Geosci. Remote Sens. Lett.*, vol. 3, no. 3, pp. 429–433, Jul. 2006.
- [13] P. Rizzoli, B. Bräutigam, T. Kraus, M. Martone, and G. Krieger, "Relative height error analysis of TanDEM-X elevation data," *ISPRS J. Photogrammetry Remote Sens.*, vol. 73, pp. 30–38, 2012.
- [14] D. Borla Tridon *et al.*, "TanDEM-X: DEM acquisition in the third year era," *Int. J. Space Sci. Eng.*, vol. 1, no. 4, pp. 367–381, 2014.
- [15] P. Rizzoli, M. Martone, and B. Bräutigam, "Global interferometric coherence maps from TanDEM-X Quicklook Data," *IEEE Geosci. Remote Sens. Lett.*, vol. 11, no. 11, pp. 1861–1865, Nov. 2014.
- [16] M. Martone, B. Bräutigam, and G. Krieger, "Quantization effects in TanDEM-X data," *IEEE Trans. Geosci. Remote Sens.*, vol. 53, no. 2, pp. 583–597, Feb. 2015.
- [17] M. Martone, B. Bräutigam, P. Rizzoli, C. Gonzalez, M. Bachmann, and G. Krieger, "Coherence evaluation of TanDEM-X interferometric data," *ISPRS J. Photogrammetry Remote Sens.*, vol. 73, pp. 21–29, 2012.
- [18] M. Martone, B. Bräutigam, and G. Krieger, "Decorrelation effects in bistatic TanDEM-X data," in *Proc. Int. Geosci. Remote Sens. Symp.*, 2012, pp. 5558–5561.
- [19] M. Martone, P. Rizzoli, and G. Krieger, "Volume decorrelation effects in TanDEM-X interferometric SAR data," *IEEE Geosci. Remote Sens. Lett.*, vol. 13, no. 12, pp. 1812–1816, Dec. 2016.
- [20] F. De Zan, G. Krieger, and F. López-Dekker, "On some spectral properties of TanDEM-X interferograms over forested areas," *IEEE Geosci. Remote Sens. Lett.*, vol. 10, no. 1, pp. 71–75, Jan. 2013.
- [21] M. Martone, B. Bräutigam, P. Rizzoli, N. Yague-Martinez, and G. Krieger, "Enhancing interferometric SAR performance over sandy areas: Experience from the TanDEM-X mission," *IEEE J. Sel. Topics Appl. Earth Observ. Remote Sens.*, vol. 9, no. 3, pp. 1036–1046, Mar. 2016.
- [22] M. Martone, B. Bräutigam, P. Rizzoli, and G. Krieger, "TanDEM-X performance over sandy areas," in *Proc. Eur. Conf. Synthetic Aperture Radar*, 2014, pp. 1–4.
- [23] M. Lachaise, T. Fritz, and M. Eineder, "Dual-baseline phase unwrapping challenges in the TanDEM-X mission," in *Proc. Eur. Conf. Synthetic Aperture Radar*, 2014, pp. 1129–1132.
- [24] M. Lachaise, T. Fritz, and R. Bamler, "The dual-baseline phase unwrapping correction framework for the TanDEM-X Mission Part 1: Theoretical description and algorithms," *IEEE Trans. Geosci. Remote Sens.*, vol. 56, no. 2, pp. 780–798, Feb. 2018.
- [25] M. Lachaise, T. Fritz, and H. Breit, "InSAR processing and dual-baseline phase unwrapping for global TanDEM-X DEM generation," in *Proc. IEEE Geosci. Remote Sens. Symp. (IGARSS)*, 2014, pp. 2229–2232.
- [26] M. Bachmann *et al.*, "TanDEM-X acquisition status and calibration of the interferometric system," in *Proc. Int. Geosci. Remote Sens. Symp.*, 2012, pp. 1900–1903.
- [27] M. Zink, M. Bartusch, and D. Ulrich, "TanDEM-X Mission Status," in *Proc. Eur. Conf. Synthetic Aperture Radar*, 2012, pp. 1–4.
- [28] B. Bräutigam *et al.*, "TanDEM-X acquisition and quality overview with two global coverages," in *Proc. Int. Geosci. Remote Sens. Symp.*, 2013, pp. 2958–2961.
- [29] M. Zink and A. Moreira, "TanDEM-X mission: Overview, challenges and status," in *Proc. Int. Geosci. Remote Sens. Symp.*, 2013, pp. 1885–1888.
- [30] T. Kraus, M. Bachmann, P. Rizzoli, B. Bräutigam, and G. Krieger, "TanDEM-X performance: Impact on acquisition planning optimization," in *Proc. Int. Radar Symp.*, 2012, pp. 371–375.
- [31] B. Bräutigam *et al.*, "TanDEM-X Global DEM quality status and acquisition completion," in *Proc. Int. Geosci. Remote Sens. Symp.*, 2014, pp. 3390–3393.
- [32] D. Schulze *et al.*, "Status of TanDEM-X DEM acquisition, calibration and performance," in *Proc. Eur. Conf. Synthetic Aperture Radar*, 2014, pp. 1–4.
- [33] M. Zink and A. Moreira, "TanDEM-X mission status: The new topography of the Earth takes shape," in *Proc. Int. Geosci. Remote Sens. Symp.*, 2014, pp. 3386–3389.
- [34] M. Bachmann, B. Bräutigam, D. Schulze, G. Krieger, and M. Zink, "TanDEM-X acquisition plan and DEM performance in the third year of operation," in *Proc. Asia-Pacific Conf. Synthetic Aperture Radar*, 2013, pp. 12–15.
- [35] M. Zink, "TanDEM-X: Key features and mission status," in *Proc. Eur. Conf. Synthetic Aperture Radar*, 2014, pp. 759–762.
- [36] M. Bachmann *et al.*, "TanDEM-X acquisition status DEM performance," in *Proc. TerraSAR-X /TanDEM-X Sci. Team Meeting*, 2013.
- [37] M. Martone, B. Bräutigam, P. Rizzoli, and G. Krieger, "Impact of SAR raw data quantization on TanDEM-X performance," in *Proc. Int. Geosci. Remote Sens. Symp.*, 2013, pp. 4487–4490.
- [38] B. Bräutigam, M. Martone, P. Rizzoli, M. Bachmann, and G. Krieger, "Interferometric performance of TanDEM-X Global DEM acquisitions," in *Proc. Eur. Conf. Synthetic Aperture Radar*, 2012, pp. 89–92.
- [39] P. Rizzoli, M. Bachmann, and B. Bräutigam, "Global performance monitoring from TanDEM-X Quicklook data," in *Proc. Eur. Conf. Synthetic Aperture Radar*, 2012, pp. 501–504.
- [40] D. Schulze, M. Bachmann, D. Borla Tridon, M. Zink, and G. Krieger, "TanDEM-X acquisition planning and DEM performance in the third year of operation," in *Proc. CSA ASAR Workshop*, 2013.
- [41] D. Borla Tridon *et al.*, "TanDEM-X DEM difficult terrain & antarctica acquisitions towards the planning of the science phase," in *Proc. Eur. Conf. Synthetic Aperture Radar*, 2014, pp. 1133–1136.
- [42] D. Borla Tridon *et al.*, "TanDEM-X Going for the DEM: Acquisition, performance, and further activities," in *Proc. Asia-Pac. Conf. Synthetic Aperture Radar*, 2015.
- [43] C. Rossi, F.R. Gonzalez, T. Fritz, N. Yague-Martinez, and M. Eineder, "TanDEM-X calibrated raw DEM generation," *ISPRS J. Photogrammetry Remote Sens.*, vol. 73, pp. 12–20, 2012.
- [44] B. Schutz, H. Zwally, C. Shuman, D. Hancock, and J. Di Marzio, "Overview of the ICESat mission," *Geophys. Res. Lett.*, to be published, doi: [32.10.1029/2005GL02400](https://doi.org/10.1029/2005GL02400).
- [45] S. Zhu, C. Reigber, and R. Koenig, "Integrated adjustment of CHAMP, GRACE, and GPS data," *J. Geodesy*, vol. 78, pp. 103–108, 2004.
- [46] M. Wermuth, O. Montenbruck, and A. Wendleder, "Relative navigation for the TanDEM-X mission and evaluation with DEM calibration results," in *Proc. Int. Symp. Spaceflight Dyn.*, 2011, pp. 28–38.
- [47] R. Dach, U. Hugentobler, P. Fridez, and M. Meindl, "Bernese GPS software version 5.0," *Astronomical Inst., Univ. Bern, Bern, Switzerland*, 2007.
- [48] J. Hueso González *et al.*, "Bistatic system and baseline calibration in TanDEM-X to ensure the global digital elevation model quality," *ISPRS J. Photogrammetry Remote Sens.*, vol. 38, pp. 3–11, 2012.
- [49] J. Walter Antony, J. Hueso González, M. Schwerdt, M. Bachmann, G. Krieger, and M. Zink, "Results of the TanDEM-X baseline calibration," *IEEE J. Sel. Topics Appl. Earth Observ. Remote Sens.*, vol. 6, no. 3, pp. 1495–1501, Jun. 2013.
- [50] M. Bachmann, J. Hueso Gonzalez, G. Krieger, M. Schwerdt, J. Walter Antony, and F. De Zan, "Calibration of the bistatic TanDEM-X interferometer," in *Proc. Eur. Conf. Synthetic Aperture Radar*, 2012, pp. 97–100.
- [51] G. Krieger and F. de Zan, "Relativistic effects in bistatic synthetic aperture radar," *IEEE Trans. Geosci. Remote Sens.*, vol. 52, no. 2, pp. 1480–1488, Feb. 2014.
- [52] T. Fritz, H. Breit, C. Rossi, U. Balss, M. Lachaise, and U. Duque, "Interferometric processing and products of the TanDEM-X mission," in *Proc. Int. Geosci. Remote Sens. Symp.*, 2012, pp. 1904–1907.
- [53] B. Wessel *et al.*, "Design of the DEM mosaicking and calibration processor for TanDEM-X," in *Proc. Eur. Conf. Synthetic Aperture Radar*, 2008, pp. 111–114.
- [54] T. Fritz, H. Breit, N. Adam, M. Eineder, and M. Lachaise, "Interferometric SAR processing: From TerraSAR-X to TanDEM-X," in *Proc. Eur. Conf. Synthetic Aperture Radar*, 2008, pp. 1–4.
- [55] H. Breit, T. Fritz, U. Balss, M. Lachaise, A. Niedermeier, and M. Vonavka, "TerraSAR-X SAR processing and products," *IEEE Trans. Geosci. Remote Sens.*, vol. 48, no. 2, pp. 727–740, Feb. 2010.
- [56] U. Balss, A. Niedermeier, and H. Breit, "TanDEM-X bistatic SAR processing," in *Proc. Eur. Conf. Synthetic Aperture Radar*, 2010, pp. 751–754.
- [57] N. Yague-Martinez and M. Eineder, "TanDEM-X mission: SAR image coregistration aspects," in *Proc. Eur. Conf. Synthetic Aperture Radar*, 2010, pp. 576–579.

- [58] M. Lachaise, T. Fritz, U. Balss, R. Bamler, and M. Eineder, "Phase unwrapping correction with dual-baseline data for the TanDEM-X mission," in *Proc. Int. Geosci. Remote Sens. Symp.*, 2012, pp. 5566–5569.
- [59] M. Lachaise, U. Balss, T. Fritz, and H. Breit, "The dual-baseline interferometric processing chain for the TanDEM-X mission," in *Proc. Int. Geosci. Remote Sens. Symp.*, 2012, pp. 5562–5565.
- [60] C. Rossi, M. Eineder, T. Fritz, and H. Breit, "TanDEM-X mission: Raw DEM generation," in *Proc. Eur. Conf. Synthetic Aperture Radar*, 2010, pp. 146–149.
- [61] G. Krieger, F. De Zan, M. Bachmann, J. Hueso Gonzalez, M. Rodriguez Cassola, and M. Zink, "Unexpected height offsets in TanDEM-X: Explanation and correction," in *Proc. Int. Geosci. Remote Sens. Symp.*, 2012, pp. 295–298.
- [62] M. Huber *et al.*, "Ensuring Globally the TanDEM-X height accuracy: Analysis of the reference data sets ICESat, SRTM, and KGPS-tracks," in *Proc. Int. Geosci. Remote Sens. Symp.*, 2009, pp. 769–772.
- [63] A. Gruber, B. Wessel, M. Huber, and A. Roth, "Operational TanDEM-X DEM calibration and first validation results," *ISPRS J. Photogrammetry Remote Sens.*, vol. 38, pp. 39–49, 2012.
- [64] A. Gruber, B. Wessel, M. Martone, and A. Roth, "The TanDEM-X DEM mosaicking: Fusion of multiple acquisitions using InSAR quality parameters," *IEEE J. Sel. Topics Appl. Earth Observ. Remote Sens.*, vol. 9, no. 3, pp. 1047–1057, Mar. 2016.
- [65] B. Wessel, "TanDEM-X Ground Segment – DEM Products Specification Document," Public Document TD-GS-PS-0021, Issue 3.0, 2013.
- [66] P. Rizzoli *et al.*, "Generation and performance assessment of the global TanDEM-X digital elevation model," *ISPRS J. Photogrammetry Remote Sens.*, vol. 73, pp. 119–139, 2017.
- [67] C. Wecklich, C. Gonzalez, and B. Bräutigam, "Height accuracy for the first part of the global TanDEM-X DEM data," in *Proc. Geomorphometry*, 2015.
- [68] C. Wecklich, C. Gonzalez, B. Bräutigam, and P. Rizzoli, "Height accuracy and data coverage status of the global TanDEM-X DEM," in *Proc. Eur. Conf. Synthetic Aperture Radar*, 2016, pp. 1–4.
- [69] P. Rizzoli, B. Bräutigam, T. Kraus, M. Martone, and G. Krieger, "Relative height error analysis of TanDEM-X elevation data," *ISPRS J. Photogrammetry Remote Sens.*, vol. 73, pp. 30–38, 2012.
- [70] P. Rizzoli, M. Martone, and B. Bräutigam, "Global mosaics of the relative height error from TanDEM-X Quicklooks," *IEEE Geosci. Remote Sens. Lett.*, vol. 12, no. 9, pp. 1928–1932, Sep. 2015.
- [71] C. Gonzalez and B. Bräutigam, "Relative height accuracy estimation method for InSAR-based DEMs," *IEEE J. Sel. Topics Appl. Earth Observ. Remote Sens.*, vol. 8, no. 11, pp. 5352–5360, Nov. 2015.
- [72] C. Gonzalez, B. Bräutigam, and P. Rizzoli, "Relative height accuracy analysis of TanDEM-X DEM products," in *Proc. Eur. Conf. Synthetic Aperture Radar*, 2016, pp. 1–4.
- [73] C. Gonzalez *et al.*, "The new global digital elevation model: TanDEM-X DEM and its final performance," in *Proc. Eur. Geosci. Union Gen. Assembly*, 2017.
- [74] C. Wecklich, C. Gonzalez, and P. Rizzoli, "TanDEM-X height performance and data coverage," in *Proc. Int. Geosci. Remote Sens. Symp.*, 2017, pp. 4088–4091.
- [75] B. Wessel, M. Huber, C. Wohlfart, U. Marschalk, D. Kosmann, and A. Roth, "Accuracy assessment of the Global TanDEM-X digital elevation model with GPS data," *ISPRS J. Photogrammetry Remote Sens.*, vol. 139, pp. 171–182, 2018.
- [76] L. Hawker, J. Neal, and P. Bates, "Accuracy assessment of the TanDEM-X 90 digital elevation model for selected floodplain sites," *Remote Sens. Environ.*, vol. 232, 2019, Art. no. 111319.
- [77] D. I. Vassilaki and A. A. Stamos, "TanDEM-X DEM: Comparative performance review employing LIDAR data and DSMs," *ISPRS J. Photogrammetry Remote Sens.*, vol. 160, pp. 33–50, 2020.
- [78] P. Rizzoli *et al.*, "Performance assessment of the global TanDEM-X digital elevation model," in *Proc. CEOS SAR CalVal Workshop*, 2017.
- [79] J.-L. B. Bello *et al.*, "TanDEM-X mission status and final DEM performance," in *Proc. Int. Radar Symp.*, 2016.
- [80] WorldDEM™. Accessed: Sep. 16, 2020. [Online]. Available: <https://www.intelligence-airbusds.com/elevation-models/last>
- [81] Copernicus DEM - ESA. Accessed: Sep. 23, 2020. [Online]. Available: <https://spacedata.copernicus.eu/web/cscda/data-offer/core-datasets>
- [82] M. Martone *et al.*, "The global forest/non-forest map from TanDEM-X interferometric SAR data," *Remote Sens. Environ.*, vol. 205, pp. 352–373, 2018.
- [83] T. Esch *et al.*, "Urban footprint processor – fully automated processing chain generating settlement masks from global data of the TanDEM-X mission," *IEEE Geosci. Remote Sens. Lett.*, vol. 10, no. 6, pp. 1617–1621, Nov. 2013.
- [84] O. Arino *et al.*, "Globcover: ESA service for global land cover from MERIS," in *Proc. Int. Geosci. Remote Sens. Symp.*, 2007, pp. 2412–2415.
- [85] C. González, M. Bachmann, J. L. Bueso-Bello, P. Rizzoli, and M. Zink, "A fully automatic algorithm for editing the TanDEM-X Global DEM," *Remote Sens.*, vol. 12, no. 23, 2020, Art. no. 3961.
- [86] B. Wessel *et al.*, "TanDEM-X PolarDEM 90 m of Antarctica: Generation and error characterization," *Cryosphere Discussion*, 2021. [Online]. Available: <https://doi.org/10.5194/tc-2021-19>
- [87] M. Huber, B. Wessel, A. Wendleder, J. Hoffmann, and A. Roth, "A framework for an automatic editing of TanDEM-X digital elevation models," in *Proc. Int. Geosci. Remote Sens. Symp.*, 2015, pp. 3826–3829.
- [88] S. Abdullahi, B. Wessel, M. Huber, A. Wendleder, A. Roth, and C. Kuenzer, "Estimating penetration-related X-Band InSAR elevation bias: A study over the Greenland Ice sheet," *Remote Sens.*, vol. 11, no. 24, pp. 2072–4292, 2019.
- [89] M. Lachaise, M. Bachmann, T. Fritz, M. Huber, B. Schweißhelm, and B. Wessel, "Generations of the TanDEM-X change DEM from the new global acquisitions (2017–2019)," in *Proc. Int. Geosci. Remote Sens. Symp.*, 2019, pp. 4480–4483.
- [90] M. Lachaise, B. Schweißhelm, and T. Fritz, "The new Tandem-X change DEM: Specifications and interferometric processing," in *Proc. IEEE Latin Amer. GRSS ISPRS Remote Sens. Conf.*, 2020, pp. 646–651.
- [91] G. Krieger *et al.*, "TanDEM-X: A radar interferometer with two formation-flying satellites," *Acta Astronautica*, vol. 89, pp. 83–98, 2014.
- [92] M. Rodriguez-Cassola *et al.*, "First bistatic spaceborne SAR experiments with TanDEM-X," *IEEE Geosci. Remote Sens. Lett.*, vol. 9, no. 1, pp. 33–37, Jan. 2012.
- [93] P. Lopez-Dekker, P. Prats, F. De Zan, D. Schulze, G. Krieger, and A. Moreira, "TanDEM-X first DEM acquisition: A crossing orbit experiment," *IEEE Geosci. Remote Sens. Lett.*, vol. 8, no. 5, pp. 943–947, Sep. 2011.
- [94] R. Kahle, H. Runge, J.-S. Ardaens, S. Suchandt, and R. Romeiser, "Formation flying for along-track interferometric oceanography – First in-flight demonstration with TanDEM-X," *Acta Astronautica*, vol. 99, pp. 130–142, 2014.
- [95] M. Pinheiro, A. Reigber, and A. Moreira, "Large-baseline InSAR for precise topographic mapping: A framework for TanDEM X large-baseline data," *Adv. Radio Sci.*, vol. 15, pp. 231–241, 2017.
- [96] M. Pardini, A. Torano Caicoya, F. Kugler, and K. Papatthanassiou, "Estimating and understanding vertical structure of forests from multibaseline TanDEM X Pol-InSAR data," in *Proc. IEEE Int. Geosci. Remote Sens. Symp.*, Jul. 2013, pp. 4344–4347.
- [97] M. Nannini, M. Martone, P. Rizzoli, P. Prats Iraola, M. Rodríguez Cassola, and A. Moreira, "Spaceborne demonstration of coherent SAR tomography for future companion satellite SAR missions," in *Proc. IEEE Int. Geosci. Remote Sens. Symp.*, 2017, pp. 129–132.
- [98] F. Kugler, D. Schulze, I. Hajnsek, H. Pretzsch, and K. P. Papatthanassiou, "TanDEM-X Pol-InSAR performance for forest height estimation," *IEEE Trans. Geosci. Remote Sens.*, vol. 52, no. 10, pp. 6404–6422, Oct. 2014.
- [99] R. Romeiser, H. Runge, S. Suchandt, R. Kahle, C. Rossi, and P. S. Bell, "Quality assessment of surface current fields from TerraSAR-X and TanDEM-X along-track interferometry and Doppler centroid analysis," *IEEE Trans. Geosci. Remote Sens.*, vol. 52, no. 5, pp. 2759–2772, May 2014.
- [100] J. Mittermayer, S. Wollstadt, P. Prats Iraola, F. López-Dekker, G. Krieger, and A. Moreira, "Bidirectional SAR imaging mode," *IEEE Trans. Geosci. Remote Sens.*, vol. 51, no. 1, pp. 601–614, Jan. 2013.
- [101] F. López-Dekker *et al.*, "Experimental bidirectional SAR ATI acquisitions ocean surface with TanDEM X," in *Proc. 10th Eur. Conf. Synthetic Aperture Radar*, Jun. 2014, pp. 1–4.
- [102] A. Alonso-González, H. Joerg, K. Papatthanassiou, and I. Hajnsek, "Dual-polarimetric agricultural change analysis of long baseline TanDEM-X time series data," in *Proc. IEEE Int. Geosci. Remote Sens. Symp.*, 2016, pp. 325–328.
- [103] J. Kim, M. Younis, A. Moreira, and W. Wiesbeck, "A novel OFDM chirp waveform scheme for use of multiple transmitters in SAR," *IEEE Geosci. Remote Sens. Lett.*, vol. 10, no. 3, pp. 568–572, May 2013.
- [104] T. Kraus, B. Bräutigam, M. Bachmann, and G. Krieger, "Multistatic SAR imaging: First results of a four phase center experiment with TerraSAR X and TanDEM X," in *Proc. Eur. Conf. Synthetic Aperture Radar*, Jun. 2016, pp. 638–642.

- [105] T. Kraus *et al.*, "A unique platform to demonstrate the capabilities of distributed SAR satellite systems," in *Proc. ONERA-DLR Aerosp. Symp.*, Jun. 2016.
- [106] R. Scheiber, F. De Zan, P. Prats, L. S. A. Araujo, M. Künemund, and L. Marotti, "Interferometric sea ice mapping with TanDEM-X: First experiments," in *Proc. IEEE Int. Geosci. Remote Sens. Symp.*, 2011, pp. 3594–3597.
- [107] A. T. Caicoya, F. Kugler, I. Hajnsek, and K. P. Papathanassiou, "Large-scale biomass classification in boreal forests with TanDEM-X data," *IEEE Trans. Geosci. Remote Sens.*, vol. 54, no. 10, pp. 5935–5951, Oct. 2016.
- [108] S. V. Baumgartner, and G. Krieger, "Dual-platform large along-track baseline GMTI," *IEEE Trans. Geosci. Remote Sens.*, vol. 54, no. 3, pp. 1554–1574, Mar. 2016.
- [109] N. Yague-Martinez, P. Prats-Iraola, T. Kraus, S. Wollstadt, and R. Scheiber, "Experimental validation with TerraSAR-X/TanDEM-X of advanced interferometric modes for accurate retrieval of azimuthal displacements," in *Proc. IEEE Int. Geosci. Remote Sens. Symp.*, 2016, pp. 1444–1447.
- [110] N. Yague-Martinez, P. Prats-Iraola, S. Wollstadt, and A. Moreira, "The 2-Look TOPS mode: Design and demonstration with TerraSAR-X," *IEEE Trans. Geosci. Remote Sens.*, vol. 57, no. 10, pp. 7682–7703, Oct. 2019.
- [111] W. Abdel Jaber, He. Rott, D. Floricioiu, J. Wuite, and N. Miranda, "Heterogeneous spatial and temporal pattern of surface elevation change and mass balance of the Patagonian ice fields between 2000 and 2016," *Cryosphere*, vol. 13, pp. 2511–2535, 2019.
- [112] P. Bernhard, S. Zwieback, S. Leinss, and I. Hajnsek, "Mapping retrogressive thaw slumps using single-pass TanDEM-X observations," *IEEE J. Sel. Topics Appl. Earth Observ. Remote Sens.*, vol. 13, pp. 3263–3280, Jun. 2020.
- [113] T. G. Yitayew *et al.*, "Validation of sea-ice topographic heights derived from TanDEM-X interferometric SAR data with results from laser profiler and photogrammetry," *IEEE Trans. Geosci. Remote Sens.*, vol. 56, no. 11, pp. 6504–6520, Nov. 2018.
- [114] P. Milillo *et al.*, "Heterogeneous retreat and ice melt of Thwaites Glacier, West Antarctica," *Sci. Adv.*, vol. 5, no. 1, Jan. 2019, Art. no. eaau3433, doi: [10.1126/sciadv.aau3433](https://doi.org/10.1126/sciadv.aau3433).
- [115] C. Sommer, P. Malz, T. C. Seehaus, S. Lippl, M. Zemp, and M. H. Braun, "Rapid glacier retreat and downwasting throughout the European Alps in the early 21st century," *Nature Commun.*, vol. 11 2020, Art. no. 3209.
- [116] A. Moreira *et al.*, "Tandem L: A highly innovative bistatic SAR mission for global observation of dynamic processes on the Earth's surface," *IEEE Geosci. Remote Sens. Mag.*, vol. 3, no. 2, pp. 8–23, Jun. 2015.
- [117] M. Davidson *et al.*, Copernicus L-band SAR mission requirements document, Issue 2.0, 10.10, 2018. [Online]. Available: https://esamultimedia.esa.int/docs/EarthObservation/Copernicus_L-band_SAR_mission_ROSE-L_MRD_v2.0_issued.pdf
- [118] M. D'Errico, *Distributed Space Missions for Earth System Monitoring*. New York, NY, USA: Springer, 2013.
- [119] G. Krieger, I. Hajnsek, K. Papathanassiou, M. Younis, and A. Moreira, "Interferometric Synthetic Aperture Radar (SAR) missions employing formation flying," *Proc. IEEE*, vol. 98, no. 5, pp. 816–843, May 2010.
- [120] A.E. Nuncio Quiroz, and M. Bartusch, "Next generation of the German X-Band SAR: The multi-static high resolution wide swath mission," in *Proc. ESA Living Planet Symp.*, May 2019.
- [121] G. Krieger *et al.*, "MirrorSAR: A fractionated space transponder concept for the implementation of low-cost multistatic SAR missions," in *Proc. Eur. Conf. Synthetic Aperture Radar*, 2018, pp. 1359–1364.



Manfred Zink received the Dipl.-Ing. degree in physics from the Technical University of Graz, Graz, Austria, in 1987, and the Dr.-Ing. degree from the University of Stuttgart, Stuttgart, Germany, in 1993.

In 1988, he joined the Microwave and Radar Institute, German Aerospace Center (DLR). He has pioneered the calibration techniques for both air- and spaceborne SAR sensors. He was the Lead X-SAR Calibration Engineer for both SIR-C/X-SAR missions in 1994 and for the SRTM mission in 2000. In August 2000, he joined the European Space Agency

(ESA) and took over the responsibility for the calibration/validation of the ASAR onboard ENVISAT. After successful in-orbit commissioning of the ASAR, he was appointed as the Principal System Engineer for ESA's TerraSAR-L Program. In May 2005, he returned to DLR's Microwaves and Radar Institute, where he is currently heading the Satellite SAR Systems Department. From 2006 to 2015 he was leading the TanDEM-X ground segment project. Since 1991 he has been

an active member of the CEOS Working Group on Calibration and Validation, SAR Subgroup and from 2011 to 2016 he has been chairing this group.

Mr. Zink was the recipient of the DLR Science Award, in 1991 and the EUSAR Best Paper Award, in 2008. In 2012 he and his colleagues were presented with the IEEE W.R.G. Baker Prize Paper Award and have been nominated for the German Federal President's Prize for Technology and Innovation. He was the General Chairman of the European SAR Conference (EUSAR) 2014.



Alberto Moreira (Fellow, IEEE) received the B.S.E.E. and M.S.E.E. degrees from the Aeronautical Technological Institute (ITA), São José dos Campos, Brazil, in 1984 and 1986, respectively, and the Eng. Dr. degree (Hons.) from the Technical University of Munich, Munich, Germany, in 1993.

From 1996 to 2001, he was the Head of the SAR Technology Department, German Aerospace Center (DLR), Oberpfaffenhofen, Germany. Under his leadership, the DLR airborne SAR system has been upgraded to operate in innovative imaging modes like

polarimetric SAR interferometry, tomography, and holography. Since 2001, he has been the Director of the Microwaves and Radar Institute, DLR, and a Full Professor with the Karlsruhe Institute of Technology (KIT), in the field of microwave remote sensing. His DLR's Institute contributes to several scientific programs and projects for spaceborne SAR missions like TerraSAR-X, TanDEM-X, HRWS, SAR-Lupe, and SARah as well as Kompsat-6, PAZ, Sentinel-1, BIOMASS, ROSE-L, and Sentinel-1NG. The mission TanDEM-X, led by his Institute, has generated a global, high-resolution digital elevation model of the Earth with unprecedented accuracy. He is the initiator and principal investigator (PI) for this mission. His professional interests and research interests include spaceborne radar end-to-end system design, microwave techniques and system concepts, signal processing, and remote sensing applications. He has authored or coauthored more than 450 publications in international conferences and journals, 8 book chapters, and holds more than 40 international patent grants in the radar and antenna field.

Mr. Moreira has served as the President of the IEEE Geoscience and Remote Sensing (GRS) Society in 2010 as well as General Co-Chair of IGARSS in 2012. He was the Founder and Chair of the GRSS German Chapter (2003–2008), served as an Associate Editor for the IEEE GRS Letters (2003–2007) and for the IEEE TGRS (since 2005), and is serving as chair of the Major Awards of the GRS Society since 2017. He was the recipient of several international awards including the IEEE AESS Nathanson Award (1999) for the "Young Radar Engineer of the Year," the IEEE Kiyo Tomiyasu Field Award (2007), the IEEE W.R.G. Baker Award from the IEEE Board of Directors (2012), and the IEEE GRSS Distinguished Achievement Award (2014). He and his colleagues received the GRSS Transactions Prize Paper Awards in 1997, 2001, and 2007 and the GRSS Letters Prize Paper Award in 2015 and 2017. From 2012 to 2018 he has served as the Principal Investigator for the Helmholtz Alliance "Remote Sensing and Earth System Dynamics" in support of Tandem-L, a radar mission proposal for the global observation of dynamic processes on Earth's surface with unprecedented quality and resolution.



Irena Hajnsek (Fellow, IEEE) received the Diploma degree (Hons.) from the Free University of Berlin, Berlin, Germany, in 1996, and the Dr. degree (Hons.) from the Friedrich Schiller University of Jena, Jena, Germany, in 2001.

Since November 2009, she has been a Professor of Earth Observation with the Swiss Federal Institute of Technology, Zürich Institute of Environmental Engineering, Zürich, Switzerland, and, at the same time, the head of the Polarimetric SAR Interferometry Research Group with the German Aerospace Center

Microwaves and Radar Institute, Wessling, Germany. Since 2010, she has been the Science Coordinator of the German satellite mission TanDEM-X and proposed satellite mission Tandem-L. Her main research interests include electromagnetic propagation and scattering theory, radar polarimetry, SAR and interferometric SAR data processing techniques, and environmental parameter modeling and estimation.

Dr. Hajnsek was the Technical Program Co-Chair of the IEEE IGARSS 2012 in Munich, Germany, and IEEE IGARSS 2019 in Yokohama, Japan. Since 2013, she has been a member of the IEEE GRSS AdCom, and since 2016, she has been the Vice-President of the IEEE GRSS Technical Committees.



Paola Rizzoli received the bachelor's and master's degrees in telecommunication engineering from the Politecnico di Milano University (Polimi), Milan, Italy, in 2003 and 2006, respectively, and the Dr.-Ing. (Ph.D.) degree (*summa cum laude*) in electrical engineering and information technology from the Karlsruhe Institute of Technology (KIT), Karlsruhe, Germany, in 2018.

From 2006 to 2008, she was with the Politecnico di Milano and Aresys s.r.l., a Polimi spin-off company, as a Scientific Researcher and a Project Engineer. At the end of 2008, she joined the Microwaves and Radar Institute, German Aerospace Center (DLR), Oberpfaffenhofen, Germany, as a Project Engineer, where she has been involved in the development and optimization of the TerraSAR-X and TanDEM-X spaceborne SAR missions, concentrating, in particular, on the generation of the TanDEM-X global digital elevation model. From 2016 to 2020, she led the System Performance Research Group of the Satellite SAR Systems Department, being responsible for the final performance assessment of the global TanDEM-X DEM and the generation of the global TanDEM-X Forest/Non-Forest map. Her main research interests include SAR systems design, data reduction techniques, estimation theory, variable modeling, signal processing, and artificial intelligence algorithms. She has been leading the Radar Science Group, concentrating on the development of innovative machine learning- and deep learning-based approaches for the study of the biosphere and the cryosphere from remotely sensed earth observation data, ranging from land cover classification and deforestation monitoring to snow facies classification and glaciers dynamics.

Dr. Rizzoli was a recipient of the DLR Science Award, in 2018 and of the Best Paper Award at the German Microwave Conference, in 2019. She regularly serves as a Reviewer for the IEEE TRANSACTIONS ON GEOSCIENCE AND REMOTE SENSING, the IEEE GEOSCIENCE AND REMOTE SENSING LETTERS, and the IEEE JOURNAL OF SELECTED TOPICS IN APPLIED EARTH OBSERVATIONS AND REMOTE SENSING.



Markus Bachmann received the Dipl.-Ing. and Ph.D. degrees in electrical engineering from the Technical University of Karlsruhe, Karlsruhe, Germany, in 2005 and 2015, respectively.

In 2005 he joined the Microwaves and Radar Institute, German Aerospace Center. From 2005 to 2011 he was in-charge of the implementation and calibration of the TerraSAR-X/TanDEM-X antenna model. From 2006 to 2010 he assessed the potentials and methods of the DEM calibration for TanDEM-X.

From 2008 to 2010 he was responsible for the planning and execution of the TanDEM-X commissioning phase. Between 2011 and 2014 he performed the interferometric and radargrammetric calibration of the TanDEM-X system and established the monitoring of the global coverage for the TanDEM-X mission. He has been a ground segment Project Manager of the Tandem-L/Rose-L-Tandem project since 2016. Since 2012, he has been the Head of the Mission Engineering Group, which is in-charge of the operational planning of the bistatic acquisitions for TanDEM-X and for future missions like Tandem-L, Rose-L Tandem, or HRWS as well as for the analysis of mission relevant aspects in the frame of various SAR missions.



Ralph Kahle received the Dipl.-Ing. degree in aerospace engineering from the Technical University of Dresden, Dresden, Germany, in 2001, and the Dr.-Ing. degree from the Technical University of Berlin, Berlin, Germany, in 2005.

In 2004, he joined DLR's German Space Operations Center (GSOC). He is responsible for flight dynamics system engineering and operations of the missions TerraSAR-X and TanDEM-X. His field of work also comprises space mission analysis, flight dynamics software development, and project man-

agement. Since 2016 he has been heading the GSOC's Flight Dynamics Team.



Thomas Fritz received the Diploma degree in physics from the University of Münster, Münster, Germany, in 1996, and the Ph.D. degree in astronomy from the University of Bonn, Bonn, Germany, in 2000.

He had a postdoctoral position with the Radioastronomical Institute, University of Bonn. In 2003, he joined the Remote Sensing Technology Institute, German Aerospace Center (DLR), Wessling, Germany, and participated in the development of the TerraSAR-X multimode synthetic aperture radar (SAR) processor. In particular, he was responsible for the TerraSAR-X SAR product specification. Since 2008, he has been leading the development of the bistatic interferometric SAR processing chain for the TanDEM-X mission. He is currently the Leader of the team "new SAR applications" in the Remote Sensing Technology Institute and working on processing chain designs for future SAR missions. His research interests include geodetic and geophysical SAR applications, SAR- and InSAR algorithms, and SAR topography.



Martin Huber received the Dipl.-Ing. degree in geodesy from the Technical University Munich, Munich, Germany, in 2002.

He joined the German Aerospace Centre (DLR) as a Researcher at the German Remote Sensing Data Center (DFD), in 2002. He has expertise in radar image processing, with focus on ortho-rectification and image analysis. Within the TanDEM-X mission he is part of the "Mosaicking and Calibration Processor" development team, which is accountable for the final TanDEM-X DEM generation. Furthermore, he is

responsible for the maintenance and development of the Digital Elevation Model Database (DEM-DB) at the DFD. The DEM-DB supports storage, extraction, and fusion of DEMs with different resolution and quality. His research interests include SAR image processing, digital elevation models, and hydrological topics.



Gerhard Krieger (Fellow, IEEE) received the Dipl.-Ing. (M.S.) and Dr.-Ing. (Ph.D.) (Hons.) degrees in electrical and communication engineering from the Technical University of Munich, Munich, Germany, in 1992 and 1999, respectively.

From 1992 to 1999, he was with the Ludwig Maximilians University, Munich, where he conducted multidisciplinary research on neuronal modeling and nonlinear information processing in biological and technical vision systems. Since 1999, he has been with the Microwaves and Radar Institute of the German Aerospace Center (DLR), Oberpfaffenhofen, Germany, where he started

as a Research Associate developing signal processing algorithms for a novel forward-looking radar system employing digital beamforming on receive. From 2001 to 2007, he led the New SAR Missions Group which pioneered the development of advanced bistatic and multistatic radar systems, such as TanDEM-X, as well as innovative multichannel SAR techniques and algorithms for high-resolution wide-swath SAR imaging. Since 2008, he has been the Head of the Radar Concepts Department which hosts about 40 scientists focusing on new SAR techniques, missions, and applications. He has moreover been serving as a Mission Engineer for TanDEM-X and he also made major contributions to the development of the Tandem-L mission concept, where he led the Phase-0 and Phase-A studies. Since 2019, he has been a Professor with the Friedrich-Alexander-University Erlangen, Erlangen, Germany. He has authored or coauthored more than 100 peer-reviewed journal papers, 9 invited book chapters, more than 400 conference papers, and more than 20 patents.

Dr. Krieger has been an Associate Editor for the IEEE TRANSACTIONS ON GEOSCIENCE AND REMOTE SENSING since 2012. In 2014, he served as the Technical Program Chair for the European Conference on Synthetic Aperture Radar and as a Guest Editor for the IEEE JOURNAL OF SELECTED TOPICS IN APPLIED EARTH OBSERVATIONS AND REMOTE SENSING. He was the recipient of several national and international awards, including two best paper awards at the European Conference on Synthetic Aperture Radar, two Transactions prize paper awards of the IEEE Geoscience and Remote Sensing Society, and the W.R.G. Baker Prize Paper Award from the IEEE Board of Directors.



Marie Lachaise received the Engineer degree in electronics, telecommunications, and computer science from CPE Lyon, Villeurbanne, France, in 2005, the M.Sc. degree in embedded systems and medical images from INSA Lyon, Villeurbanne, in 2005, and the Ph.D. degree in engineering from the Technical University of Munich, Munich, Germany, in 2015.

Since 2005, she has been employed with the DLR, Oberpfaffenhofen, Germany. She developed software and algorithms for the TerraSAR-X and TanDEM-X missions. Especially she designed the algorithms related to the interferometric processing of the multichannel data of the TanDEM-X mission such as the multibaseline phase unwrapping. Since 2012, she has been responsible for the development and integration of the enhanced interferometric TanDEM-X processor and since 2016 has been the Systems Engineer responsible for the Change DEM production. During the last few years, she also works for the VERITAS mission proposed by NASA-JPL and the TanDEM-L mission proposed by DLR.

related to the interferometric processing of the multichannel data of the TanDEM-X mission such as the multibaseline phase unwrapping. Since 2012, she has been responsible for the development and integration of the enhanced interferometric TanDEM-X processor and since 2016 has been the Systems Engineer responsible for the Change DEM production. During the last few years, she also works for the VERITAS mission proposed by NASA-JPL and the TanDEM-L mission proposed by DLR.



Michele Martone received the B.Sc. and M.Sc. degrees in telecommunication engineering from the University of Naples Federico II, Naples, Italy, in 2006 and 2009, respectively, and the Ph.D. degree from the Karlsruhe Institute of Technology, Karlsruhe, Germany, in 2019.

Since 2009, he has been with the German Aerospace Center (DLR), Microwaves and Radar Institute, Weßling, Germany, where he has been involved in the development and optimization of the TerraSAR-X and TanDEM-X spaceborne SAR missions, focusing on the generation of the global TanDEM-X digital elevation model and Forest/Non-Forest map. He has authored or coauthored nearly 90 research articles in peer-reviewed journals and international conference proceedings. His main research interests include SAR systems design, image classification, and signal processing.

Dr. Martone was the recipient of the DLR Science Award, in 2018 and of the Best Paper Award at the German Microwave Conference 2019.

Dr. Martone was the recipient of the DLR Science Award, in 2018 and of the Best Paper Award at the German Microwave Conference 2019.



Edith Maurer received the Ph.D. degree in solid state physics from the Technical University of Munich, Munich, Germany, in 2006.

In 2006 she joined the German Space Operations Center (DLR). For more than ten years she has accompanied the TerraSAR-X/TanDEM-X mission in various roles. Passing through several professional levels, starting as a mission planner, as a flight operator in satellite operations, and as a project leader on control center level he gained profound insight in the various fields of space operations.

Dr. Maurer is currently heading the Mission Operations Technology group, German Space Operations Center.



Birgit Wessel received the diploma degree in geodesy from the University of Hannover, Hanover, Germany, in 2000 and the Dr.-Ing. degree from the Technische Universitaet Muenchen (TUM), Munich, Germany, in 2006.

From 2000 to 2005, she was a Scientific Collaborator with the Institute for Photogrammetry and Cartography, TUM. Since 2005 she has been with the German Remote Sensing Data Center, German Aerospace Center (DLR), where she is currently leading the DEM calibration and mosaicking developments for the German interferometric TanDEM-X satellite mission. Her research focuses on SAR remote sensing, image analysis, and InSAR DEMs.

From 2000 to 2005, she was a Scientific Collaborator with the Institute for Photogrammetry and Cartography, TUM. Since 2005 she has been with the German Remote Sensing Data Center, German Aerospace Center (DLR), where she is currently leading the DEM calibration and mosaicking developments for the German interferometric TanDEM-X satellite mission. Her research focuses on SAR remote sensing, image analysis, and InSAR DEMs.